

AEDC-TR-75-29

cy.2

SEP 11 1975

SEP 28 1975

MAY 1 1987

6-4-97



**STATIC FORCE AND MOMENT TESTS
OF THE HOLLOMAN NARROW-GAGE ROCKET SLED
AT MACH NUMBERS FROM 1.5 TO 4.0**

**VON KÁRMÁN GAS DYNAMICS FACILITY
ARNOLD ENGINEERING DEVELOPMENT CENTER
AIR FORCE SYSTEMS COMMAND
ARNOLD AIR FORCE STATION, TENNESSEE 37389**

August 1975

Final Report for Period September 26 to October 3, 1974

Approved for public release; distribution unlimited.

Property of U. S. Air Force
PROPERTY
PROGRAM 75-0001

Prepared for

**AIR FORCE SPECIAL WEAPONS CENTER
6585TH TEST GROUP (TKE)
HOLLOMAN AFB, NEW MEXICO 88330**

NOTICES

When U. S. Government drawings specifications, or other data are used for any purpose other than a definitely related Government procurement operation, the Government thereby incurs no responsibility nor any obligation whatsoever, and the fact that the Government may have formulated, furnished, or in any way supplied the said drawings, specifications, or other data, is not to be regarded by implication or otherwise, or in any manner licensing the holder or any other person or corporation, or conveying any rights or permission to manufacture, use, or sell any patented invention that may in any way be related thereto.

Qualified users may obtain copies of this report from the Defense Documentation Center.

References to named commercial products in this report are not to be considered in any sense as an endorsement of the product by the United States Air Force or the Government.

This report has been reviewed by the Information Office (OI) and is releasable to the National Technical Information Service (NTIS). At NTIS, it will be available to the general public, including foreign nations.

APPROVAL STATEMENT

This technical report has been reviewed and is approved for publication.

FOR THE COMMANDER



JIMMY W. MULLINS
Lt Colonel, USAF
Chief Air Force Test Director, VKF
Directorate of Test



FRANK J. PASSARELLO
Colonel, USAF
Director of Test

UNCLASSIFIED

REPORT DOCUMENTATION PAGE		READ INSTRUCTIONS BEFORE COMPLETING FORM
1 REPORT NUMBER AEDC-TR-75-29	2 GOVT ACCESSION NO.	3. RECIPIENT'S CATALOG NUMBER
4 TITLE (and Subtitle) STATIC FORCE AND MOMENT TESTS OF THE HOLLOMAN NARROW-GAGE ROCKET SLED AT MACH NUMBERS FROM 1.5 TO 4.0		5 TYPE OF REPORT & PERIOD COVERED Final Report - September 26 to October 3, 1974
		6. PERFORMING ORG. REPORT NUMBER
7 AUTHOR(s) R. H. Rhudy and J. D. Corce ARO, Inc.		8. CONTRACT OR GRANT NUMBER(s)
9 PERFORMING ORGANIZATION NAME AND ADDRESS Arnold Engineering Development Center (XO) Arnold Air Force Station, Tennessee 37389		10. PROGRAM ELEMENT, PROJECT, TASK AREA & WORK UNIT NUMBERS Program Element 65807F
11 CONTROLLING OFFICE NAME AND ADDRESS Air Force Special Weapons Center 6585th Test Group (TKE) Holloman Air Force Base, New Mexico 88330		12. REPORT DATE August 1975
		13 NUMBER OF PAGES 55
14 MONITORING AGENCY NAME & ADDRESS (if different from Controlling Office)		15. SECURITY CLASS. (of this report) UNCLASSIFIED
		15a DECLASSIFICATION/DOWNGRADING SCHEDULE N/A
16 DISTRIBUTION STATEMENT (of this Report) Approved for public release; distribution unlimited.		
17. DISTRIBUTION STATEMENT (of the abstract entered in Block 20, if different from Report)		
18. SUPPLEMENTARY NOTES Available in DDC		
19 KEY WORDS (Continue on reverse side if necessary and identify by block number) static stability rocket sled supersonic flow Reynolds number aerodynamic characteristics		
20. ABSTRACT (Continue on reverse side if necessary and identify by block number) Experimental static stability and axial force data are pre- sented for several one-twelfth scale model configurations of a Narrow-Gage Dual-Rail Rocket Sled at Mach numbers from 1.5 to 4.0. The test Reynolds numbers, based on sled base diameter, varied from 0.5 to 1.4 million depending on configuration and/or Mach number. The tests were conducted with the models in close proximity to a ground plane and rail assembly simulating the High Speed Test Track at Holloman Air Force Base. Results are presented showing		

UNCLASSIFIED

UNCLASSIFIED

20. ABSTRACT (Continued)

the effects of configuration variables, such as, nose shape, water brake, water brake trough, bleed area, and sled slipper height and location.

PREFACE

The work reported herein was conducted by the Arnold Engineering Development Center (AEDC), Air Force Systems Command (AFSC), at the request of the Air Force Special Weapons Center (AFSWC), 6585th Test Group (JON 06TN2800), under Program Element 65807F. The monitor for this project was Mr. D. J. Krupovage, 6585th Test Group/TKE, Holloman AFB, New Mexico. The results were obtained by ARO, Inc. (a subsidiary of Sverdrup & Parcel and Associates, Inc.), contract operator of AEDC, AFSC, Arnold Air Force Station, Tennessee. The work was done under ARO Project No. V41A-45A. The authors of this report were R. H. Rhudy and J. D. Corce, ARO, Inc. Data reduction was completed on October 25, 1974, and the manuscript (ARO Control No. ARO-VKF-TR-75-6) was submitted for publication on January 20, 1975.

CONTENTS

	<u>Page</u>
1.0 INTRODUCTION	5
2.0 APPARATUS	
2.1 Wind Tunnel	5
2.2 Model	5
2.3 Instrumentation	6
3.0 PROCEDURE	
3.1 Test Conditions	7
3.2 Test Procedure	8
3.3 Data Precision	8
4.0 RESULTS AND DISCUSSION	10
5.0 CONCLUDING REMARKS	12
REFERENCES	12

ILLUSTRATIONS

Figure

1. Narrow-Gage Sled Model Installed in Tunnel A	13
2. Model, Sting, and Ground Plane Assembly	14
3. Model Details	15
4. Bleed Area Details	16
5. Water Brake Details	17
6. Rocket Motor Details	18
7. Typical Slipper and Rail Cross Section	19
8. Typical Effects of a Change in Slipper to Rail Clearance (Configuration 2.2.1.2.1)	20
9. Effect of Water Brake on Long Cone Configuration with Short Slippers in the Forward Position (1.3.1.2.X)	23
10. Effect of Nose Shape with the Short Slippers in the Forward Position (1.3.1.X.1)	26
11. Effect of Bleed Opening on Long Cone Configuration with Short Slippers in the Forward Position (1.3.X.2.2)	29
12. Effect of Short Slipper Locations on the Long Cone (1.X.1.2.1)	33
13. Effect of Medium Slipper Locations on the Long Cone (2.X.1.2.1)	36
14. Effect of Long Slipper Locations on the Long Cone (3.X.1.2.1)	39
15. Effect of Short Slipper Locations on the Blunt Cone (1.X.1.3.1)	42

<u>Figure</u>	<u>Page</u>
16. Effect of Slipper Height on the Long Cone with Slippers in the Forward Position (X.3.1.2.1)	45
17. Effect of Slipper Height on the Blunt Cone with Slippers in the Forward Position (X.3.1.3.1)	48
18. Effect of Water Trough and Bleed Area on Long Cone Configuration with Short Slippers in the Forward Position (1.3.X.2.2x)	51

TABLE

1. Test Summary	54
NOMENCLATURE	55

1.0 INTRODUCTION

The purpose of this investigation was to determine the static stability and axial force characteristics of Narrow-Gage Rocket Sled model in the presence of a ground plane and rail assembly simulating the High Speed Test Track (narrow gage extension) at Holloman Air Force Base. As pointed out in Ref. 1, the sled bow wave interaction with the boundary layer on the ground plane and rail surfaces differs from the actual case; however, previous investigations have shown that reasonable correlations between wind tunnel data and actual track tests can be obtained. The current data were obtained on several configurations of the Narrow-Gage sled in the 40-in. Supersonic Wind Tunnel (A) of the von Kármán Gas Dynamics Facility (VKF), over a Mach number range from 1.5 to 4.0 at free-stream unit Reynolds numbers ranging from 1.4 to 5.5 million/ft. The configuration variables were nose shape, slipper height and location, bleed area open and closed, and water brake on and off. In addition to the force and moment data, base pressures and flow field shadowgraph photographs were obtained at all test conditions at the nominal test angle of attack of zero degree.

2.0 APPARATUS

2.1 WIND TUNNEL

Tunnel A is a continuous, closed-circuit, variable density wind tunnel with an automatically driven flexible-plate nozzle and a 40- by 40-in. test section. The tunnel can be operated at Mach numbers from 1.5 to 6.0 at maximum stagnation pressures from 29 to 200 psia, respectively. Minimum operating pressures range from about one-tenth to one-twentieth of the maximum pressures. Stagnation temperatures range up to 760°R ($M_{\infty} = 6.0$).

The model may be injected into the tunnel for a test run and then retracted for a model change without interrupting the tunnel flow. In this test, however, because of model vibration problems discussed later in Section 3.2, the full inject/retract capability was not used, and the model remained in the test section during tunnel startup and shutdown.

2.2 MODEL

The Narrow-Gage Rocket Sled model and ground plane assembly, designed and fabricated by Systems Research Laboratories, is shown installed in Tunnel A in Fig. 1 and schematically in Fig. 2. The aluminum one-twelfth scale model had various configurations (Fig. 3) consisting of two nose shapes (a sharp and a blunt cone), an

aerodynamic bleed area, a water brake, three sets of air brakes and slipper struts, and three locations for the front slipper struts on the sled body. Details of the various model components are shown in Figs. 4 through 7. Because of failures incurred during the test, replacement slippers and slipper struts were fabricated by VKF. Inspection of the original parts and those fabricated by VKF showed variations in the dimensions of the slippers. The dimensions shown in Fig. 7 are the design dimensions, and the actual vertical clearance between the slippers and rail, when the rail was centered, was found to be 0.070 in., not as shown. The actual lateral clearance was not measured. The three slipper heights, measured from the sled centerline to the inside top of the slipper, were 1.508, 1.676, and 1.806 in.

The model, supported by a balance and sting, could be driven in pitch and height by motor-driven yokes attached to the sting, and in roll, by a motor attached to the rear support plate of the ground plane assembly (see Fig. 2).

A six-component strain-gage balance was used to measure the aerodynamic loading on the sled which was suspended over the rails. Fouling lights were used to indicate when contact existed between the model slippers and the rail. Carborundum[®] grit was used on the model nose to promote a turbulent layer.

2.3 INSTRUMENTATION

Tunnel A stilling chamber pressure was measured with a 15-, 60-, or 150-psid transducer referenced to a near vacuum. Based on periodic comparisons with secondary standards, the precision of these transducers (a band which includes 95 percent of the residuals) is estimated to be within ± 0.2 percent of the measured pressure. Stilling chamber temperature was measured with a copper-constantan thermocouple to a precision of $\pm 2^\circ\text{F}$ based on the thermocouple wire manufacturer's specifications.

Model forces and moments were measured with a six-component, moment-type, strain-gage balance supplied and calibrated by VKF. Before the test, static loads in each plane and combined static loads were applied to the balance to simulate the range of loads anticipated for the test. The following uncertainties represent the bands for 95 percent of the measurement residuals based on differences between the applied loads and the corresponding values calculated from the final data reduction equations:

<u>Component</u>	<u>Balance Design Loads</u>	<u>Range of Static Loads</u>	<u>Measurement Uncertainty</u>
Normal Force, lb	± 30	± 6.0	± 0.150
Pitching Moment,* in.-lb	± 66	± 10.0	± 0.330
Side Force, lb	± 15	± 1.5	± 0.075

<u>Component</u>	<u>Balance Design Loads</u>	<u>Range of Static Loads</u>	<u>Measurement Uncertainty</u>
Yawing Moment,* in.-lb	±33	± 2.5	±0.165
Rolling Moment, in.-lb	±20	± 1.0	±0.100
Axial Force, lb	±30	0 → 30.0	±0.150

*About balance forward moment bridge

The transfer distance to the model moment reference point (on model centerline at the center of the aft slipper, see Fig. 3) was measured with an estimated precision of ±0.010 in.

The base pressures were measured with 15-psid transducers referenced to a near vacuum and having full-scale calibrated ranges of 1, 5, and 15 psia. Based on periodic comparison with secondary standards, the precision of these transducers was estimated to be ±0.2 percent of full scale of the range being used.

Model flow-field shadowgraphs were obtained on all configurations to show the extent of shock interaction between the sled, rails, and ground plane.

3.0 PROCEDURE

3.1 TEST CONDITIONS

The investigation was conducted at Mach numbers from 1.5 to 4.0 at the maximum possible Reynolds number, which varied with configuration at each Mach number because of load limits on the balance. At the request of AFMDC, tests were made at two uncalibrated Mach numbers ($M_{\infty} = 1.65$ and 1.85) which were obtained using interpolated nozzle contours. A summary of the range of nominal test conditions is given below:

<u>M_{∞}</u>	<u>P_o, psia</u>	<u>T_o, °R</u>	<u>p_{∞}, psia</u>	<u>q_{∞}, psia</u>	<u>$Re_{\infty d} \times 10^{-6}$</u>
1.50	7.5-12.0	570	2.0-3.2	3.2-5.2	0.53-0.86
1.65	9.0-12.7	↓	2.0-2.8	3.8-5.3	0.61-0.87
1.75	9.1-13.0		1.7-2.4	3.7-5.2	0.59-0.86
1.85	9.1-13.3		1.5-2.2	3.5-5.2	0.58-0.86
2.00	9.2-15.7		1.2-2.0	3.3-5.6	0.55-0.95
2.25	11.1-19.4	↓	1.0-1.7	3.4-5.9	0.60-1.03
2.50	15.1-23.7	575	0.9-1.4	3.9-6.1	0.67-1.12
3.00	17.9-40.0	575	0.5-1.1	3.1-6.8	0.65-1.38
3.50	40.1-47.0	585	0.5-0.6	4.5-5.2	1.07-1.24
4.00	62.5	585	0.4	4.5	1.26

A test summary showing all configurations tested along with the nomenclature for the configuration code is given in Table 1.

3.2 TEST PROCEDURE

Normally, in the model injection sequence into the airstream (model at $\alpha = 0$), transient loads are encountered as the model traverses through the tank cavity shock wave. In most cases, these loads are small and present no problem. However, the shock system above the cavity is influenced by model size and shape, and for the present model assembly, the cavity shock was considerably stronger than normal. Furthermore the small clearance between the model slippers and the rails severely restricted the permissible model deflection, and during the first injection ($M_\infty = 2.0$), several slipper components were damaged. The test, therefore, was run with the model injected prior to tunnel startup and during tunnel shutdown. Both of these operations were accomplished at reduced pressure levels; consequently, model loads were minimal.

Prior to each test run, the rail and ground plane assembly were checked for zero yaw and found to be within ± 0.1 deg. The alignment of the sled slippers in yaw with respect to the rail was also adjusted to provide nearly uniform clearance between the slippers and the rail on the sides. After flow was established, the rail-ground plane assembly was set to zero angle of attack, (within ± 0.05 deg) by the tunnel pitch mechanism and use of an optical level for verification. The sled was then adjusted by the pitch-height yoke drives so that all slippers were clear of the rail. No major attempts were made to ensure that the clearance between the slippers and the rail was uniform for all four slippers because the time involved was quite extensive. In general, however, nominally constant clearance between the slippers and the rail was maintained over the Mach number range, once a particular configuration was set at the initial test condition. The slipper clearance was monitored during all data acquisition by use of the four "foul" lights and four closed-circuit television cameras focused on the slippers. Early in the test, the clearance between the slippers and the rail was varied within the limits possible and found to have only second-order effects on the force and moment data when compared with the effects of other configuration variables. Sled base pressures were measured and used to correct the total axial force at all test conditions.

3.3 DATA PRECISION

3.3.1 Test Conditions

Uncertainties (bands which include 95 percent of the calibration data) in the basic tunnel parameters, p_0 , T_0 , and M_∞ , were estimated from repeat calibration of the instrumentation (see Section 2.3) and from the repeatability and uniformity of the test

section flow during tunnel calibrations. These uncertainties were then used to estimate uncertainties in the other free-stream properties for the primary test conditions. No estimates can be given for $M_\infty = 1.65$ and 1.85 because, as noted in Section 3.1, detailed test section calibration data required for meaningful analysis are not available. It should be noted, however, that the contour for $M_\infty = 1.85$ was checked using a pitot-pressure rake (9 tubes) mounted on the ground plane just upstream of the sled model which gave an average Mach number of $M_\infty = 1.84 \pm 0.01$. Since both these contours had been used in a previous AFMDC sled test (Ref. 2) during which similar (planar rake) calibrations had been made, it was assumed that the $M_\infty = 1.65$ contour was equally valid.

Uncertainties in Tunnel Conditions

M_∞	M_∞	p_0 , psia	p_{00} , psia	q_∞ , psia	T_0 °R, percent
1.51	± 0.010	± 0.02	± 0.047	± 0.025	± 0.5
2.00	± 0.010	± 0.02	± 0.027	± 0.038	± 0.5
2.50	± 0.008	± 0.08	± 0.016	± 0.043	± 0.5
3.01	± 0.012	± 0.08	± 0.018	± 0.067	± 0.5

3.3.2 Aerodynamic Coefficients

The balance uncertainties listed in Section 2.3 were combined with the uncertainties in the tunnel parameters, using the Taylor series method of error propagation, to estimate the precision of the aerodynamic coefficients for the primary test conditions. The relative uncertainties listed below are for three configurations over the primary Mach number range but are considered to be typical for all configurations at all other test conditions:

Configuration	M_∞	Uncertainty, percent (\pm)			
		C_N	C_m	C_{A_t}	C_A
1.3.2.2.2	1.5	2.0	1.2	0.7	2.4
	2.0	1.9	1.2	1.2	2.2
	2.5	1.6	1.3	1.1	1.8
	3.0	1.7	1.5	1.4	2.1
1.3.1.2.1	1.5	3.4	2.2	0.9	2.2
	2.0	2.0	1.7	0.8	1.6
	2.5	2.6	3.6	0.9	1.3
	3.0	2.5	3.2	1.2	1.6
1.3.1.3.1	1.5	3.2	2.3	0.6	1.6
	2.0	2.7	2.8	0.8	1.4
	2.5	3.3	3.8	0.9	1.3
	3.0	3.4	3.8	1.2	1.5

Based on the maximum possible variation in slipper clearance with respect to the rail and the most aft forward slipper location, the sled was aligned in pitch, with respect to the rails to within ± 1.0 deg.

4.0 RESULTS AND DISCUSSION

The tests were conducted at the maximum Reynolds number consistent with the balance load limits. This technique resulted in a general increase in Reynolds number as Mach number was increased and some variation with configuration changes at a given Mach number. The data presented within the report are plotted as a function of Mach number; however, there may be a second-order effect of the changing Reynolds number. The comparison of configurations at a given Mach number would be more nearly valid because, as seen in Table 1, then all configurations were tested at nearly the same Reynolds number. The data are presented in body axis coefficients. The resolution of the corresponding forces and moments into actual sled loadings on the forward and aft slipper beams on the tracks will be made by AFMDC.

As previously stated, because of the time involved, no attempt was made to maintain uniform clearance between the four slippers and the rails. Figure 8 shows the results of checks made to determine the effects of changes in slipper clearance with respect to the rail. The square symbol on the curves represents data taken in the normal manner while the bars indicate the total change measured between the condition when the model was adjusted so that the slippers were just clear of the rail on the bottom and the condition where they were just clear on the top. While there is some change in the magnitude of the stability and axial force coefficients, they are small compared with the variations with configuration presented in later figures. The calculated base axial force coefficient (C_{A_b}) for this configuration is shown in Fig. 8c. This coefficient was calculated using an average pressure from the four taps located as shown in Fig. 6. The data presented in the remainder of this report are for total axial force coefficient (C_{A_t}) because of the large variation in the base pressure measured on the four taps. An accurate base pressure correction would require a more detailed measurement of this variation.

Data are presented in Fig. 9 to show the effect of the water brake on the long cone nose configuration with short slippers. As can be seen, a substantial increase in normal force coefficient (C_N) and pitching moment coefficient (C_m) occurred when the brake was removed, while the axial force coefficient was from 5 to 11 percent higher with the brake installed. The trends with Mach number were generally the same for both configurations.

The effects of nose shape on the body axis stability coefficients (Fig. 10) are generally as would be expected if the complex interactions between the sled and ground plane are ignored. The long sharp cone produced higher normal force and sometimes higher pitching moment and a 15- to 30-percent reduction in total axial force. However at $M_\infty = 2.5$ and 3.0, pitching moment was lower for the long nose. These data were taken with the water brake installed and the slipper height and location the same for both nose shapes.

The effect of closing the bleed opening (see Fig. 4) on the long cone configuration with the brake removed is shown in Fig. 11. Closing the bleed opening decreased the normal force at the lower Mach numbers but increased normal force at $M_\infty \geq 2.0$. Pitching moment was greater, however, with the bleed closed at all Mach numbers. As seen in the schlieren photographs for $M_\infty = 3.0$ (Fig. 11c), both the upper and lower flow fields over the sled were significantly changed when the bleed area was opened. Total axial force increased at all Mach numbers (Fig. 11d) when the bleed area was opened, which can be attributed, primarily, to the additional pressure drag on the face of the bleed passage.

The effect of the forward slipper location on several configurations is shown in Figs. 12 through 15. With the short strut slippers on the long cone with the water brake installed (Fig. 12), a movement of the front slippers from the forward to the aft position (positions shown in Fig. 3) resulted in a decrease in both normal force and pitching moment over most of the Mach number range, with the decrease being very large at $M_\infty \lesssim 2.0$ particularly in normal force. By comparison, the change in axial force was relatively small. The results for the same nose configuration but with the medium height slipper struts in three locations were somewhat mixed, but generally C_N and C_m were higher for the forward location. Axial force was generally higher for the aft slipper location. There was little difference in C_N between the forward and aft location for these medium height slipper struts at $M_\infty \lesssim 1.75$, which is in marked contrast to the wide spread obtained with the short struts in Fig. 12. Although a complete set of data was not obtained with the long slipper struts installed on this configuration, the data presented in Fig. 14 indicate that, when the sled is moved further away from the ground, the effect of slipper location on the coefficients was much less pronounced over the Mach number range. The data presented in Fig. 15 for the blunt nose when compared with those of Fig. 12 indicate that the effects of slipper location were very similar for both nose shapes.

Data are presented in Figs. 16 and 17 to show the effect of a change in slipper strut height on the data obtained for the two nose shapes tested. These data were taken with the forward slipper at the most forward position and the water brake installed. These

results show that the effect of the slipper height was rather mixed below $M_\infty = 2$, but above $M_\infty = 2$, the longer slipper struts produced the higher sled forces and moments on both nose shapes.

The data presented in Fig. 18 are for the long cone with the short slippers in the forward position. These data are presented to show the effect of the water brake trough, filled and empty, on this configuration with the bleed area open and closed. The data again show a reversal in the effect above and below $M_\infty = 2$. Filling the trough in general caused a decrease or a small change in normal force and pitching moment at Mach numbers below 2; however, the opposite was generally true above $M_\infty = 2$. This effect was the same for the bleed area open or closed. Filling the water brake trough had a relatively small effect on the total axial force coefficients.

5.0 CONCLUDING REMARKS

Static force and moment tests were conducted on several configurations of the Narrow-Gage Rocket Sled at Mach numbers from 1.5 to 4.0. Based on the results presented for $M_\infty = 1.5$ to 3.0, the following observations are noted:

1. The general effect of adding the water brake on the long cone sled was to decrease the normal force and pitching moment while increasing the axial force.
2. Increasing the nose bluntness caused a decrease in normal force and pitching moment and an increase in axial force.
3. The changes in normal force and pitching moment caused by bleed area open or closed, slipper height, forward slipper location, or brake trough open and closed were, in general, opposite below and above $M_\infty \approx 2$.

REFERENCES

1. Strike, W. T. and Lucas, E. J. "Evaluation of Wind Tunnel Tests on AFMDC Monorail Cone- and Spike-Nose Sled Configurations at Mach Numbers from 2.0 to 5.0." AEDC-TR-68-198 (AD679206), December 1968.
2. Jenke, L. M. and Lucas, E. J. "Supersonic Wind Tunnel Tests of the IDS 6208 Rocket Sled." AEDC-TR-65-98 (AD463163), May 1965.

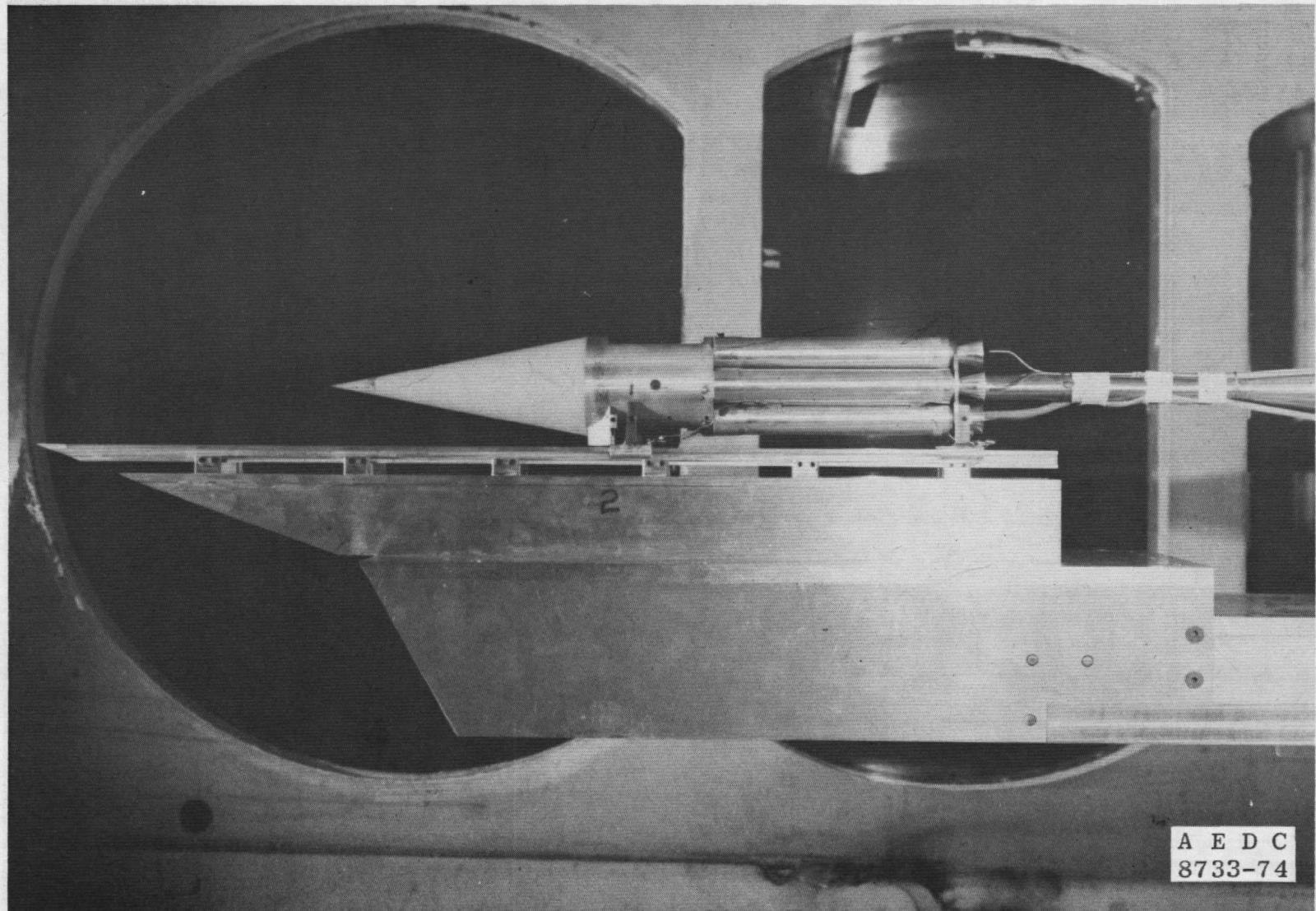


Figure 1. Narrow-gage sled model installed in Tunnel A.

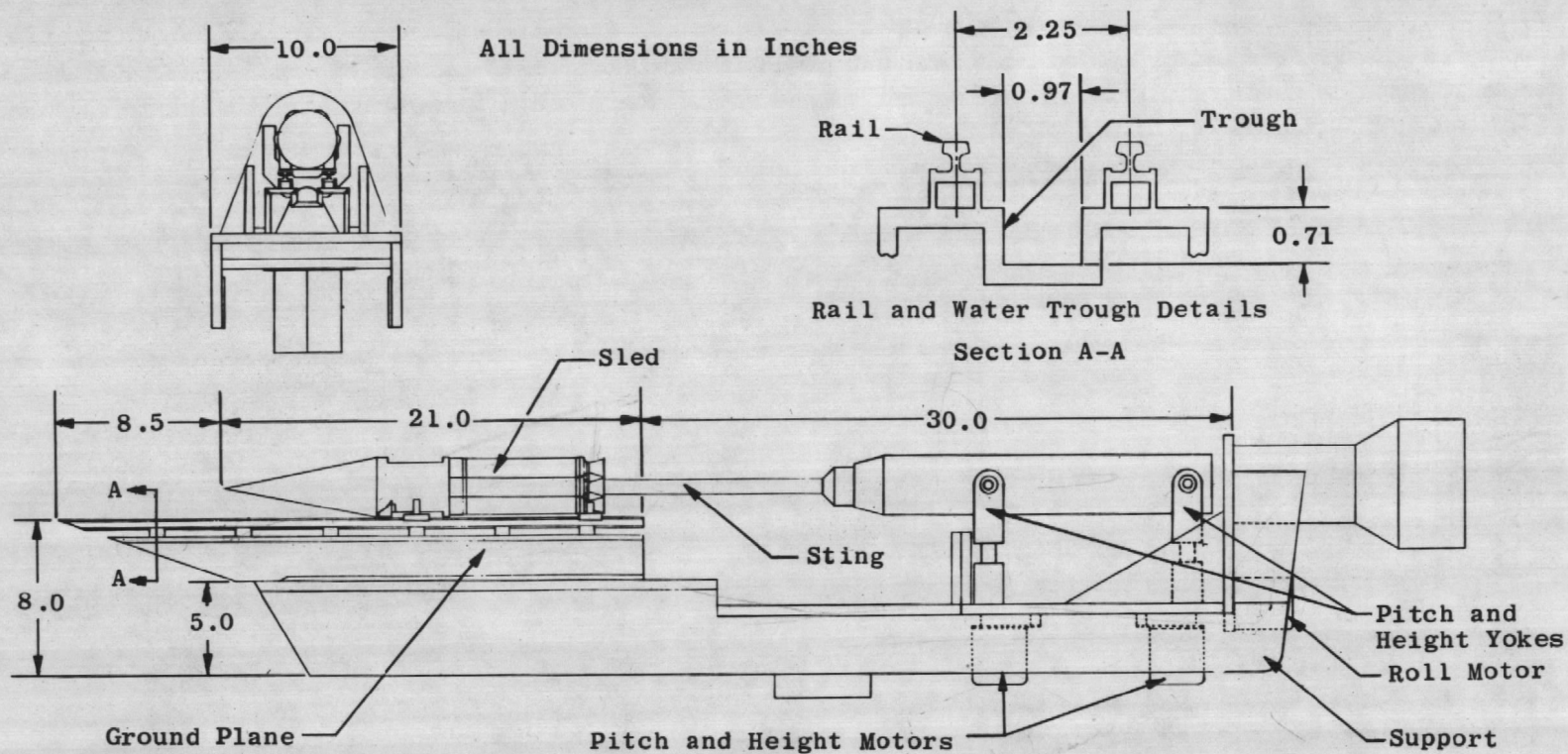


Figure 2. Model, sting, and ground plane assembly.

Slipper Heights	Dimension A
Short	1.508
Medium	1.676
Long	1.806

All Dimensions in Inches

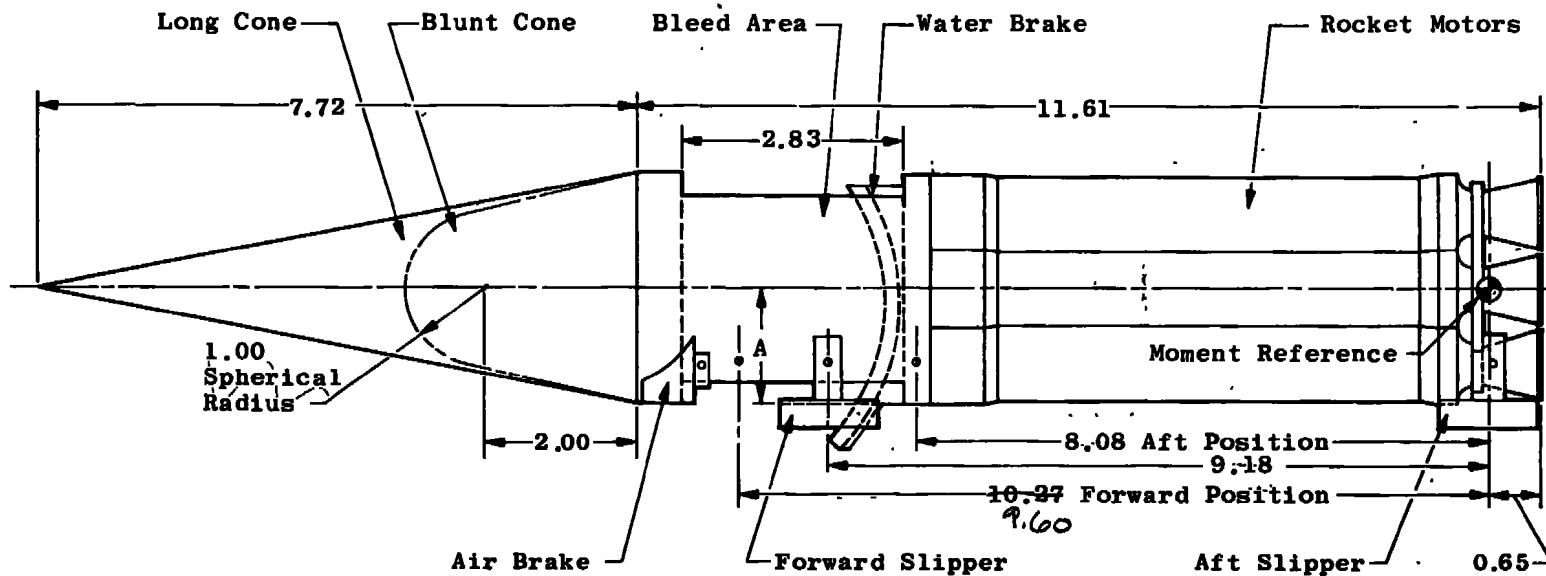
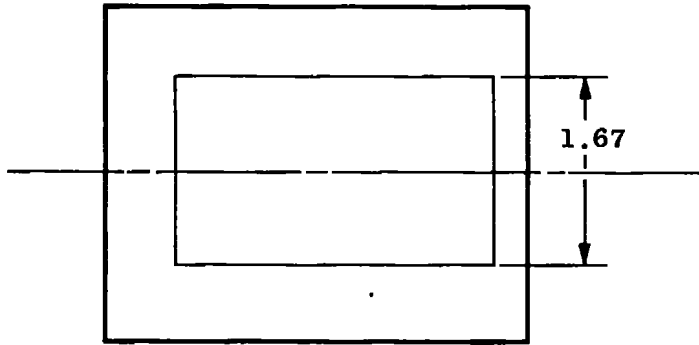
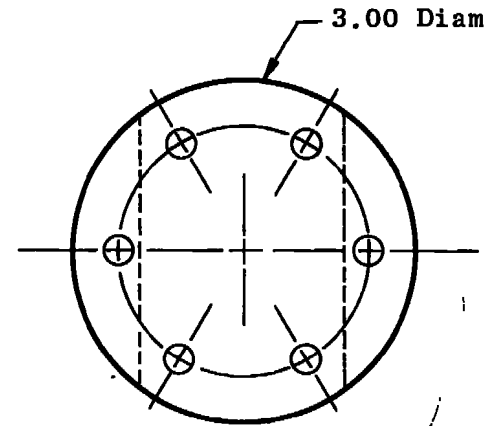
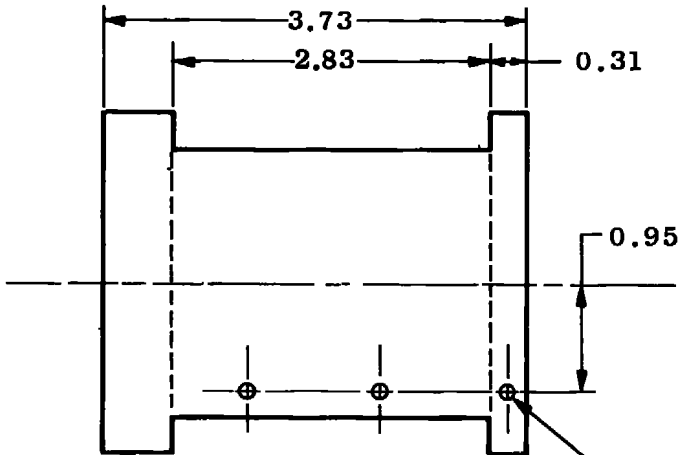


Figure 3. Model details.



All Dimensions in Inches



Slipper Strut Attachment Point (Typical) (See Also Fig. 3)

Figure 4. Bleed area details.

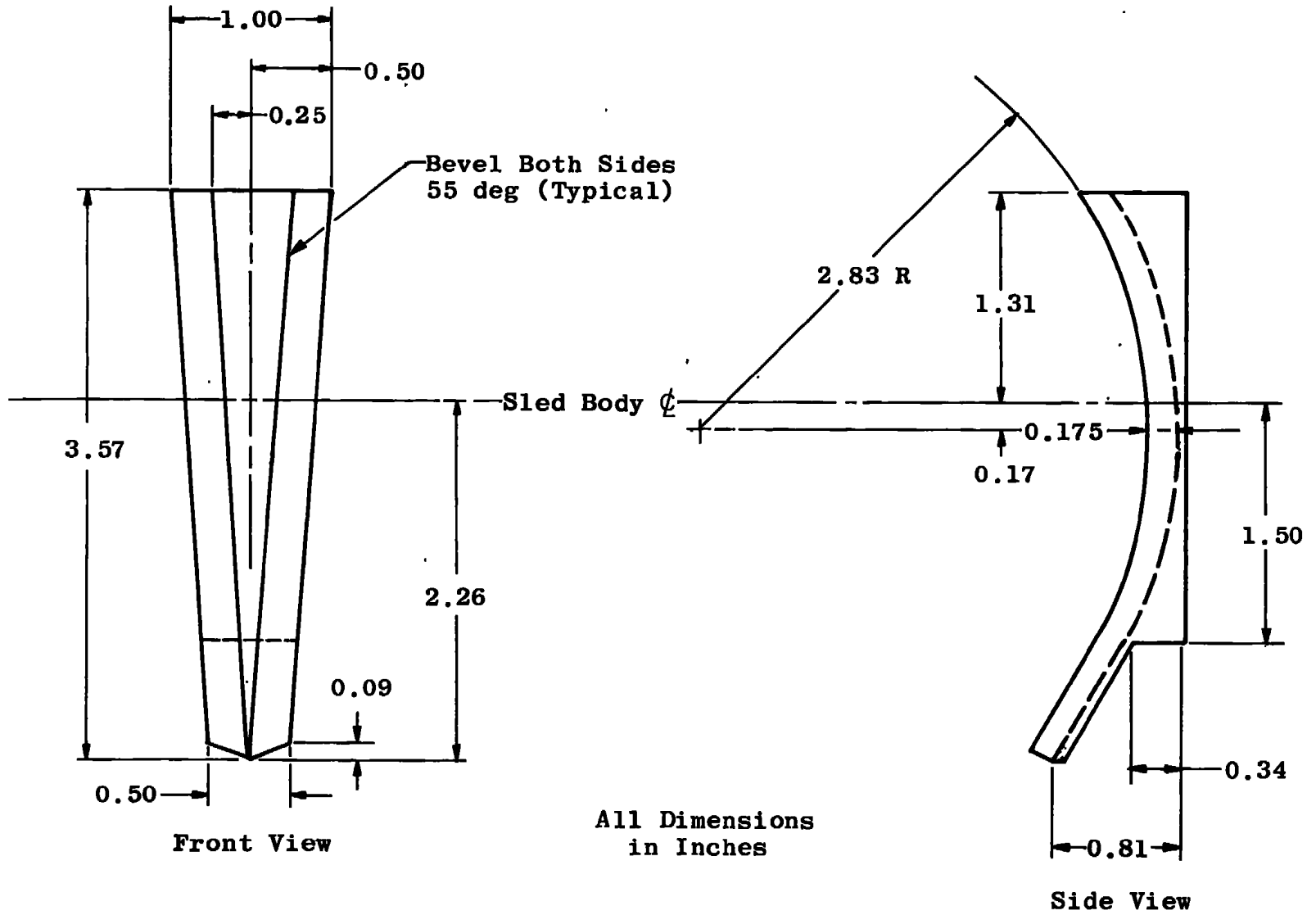


Figure 5. Water brake details.

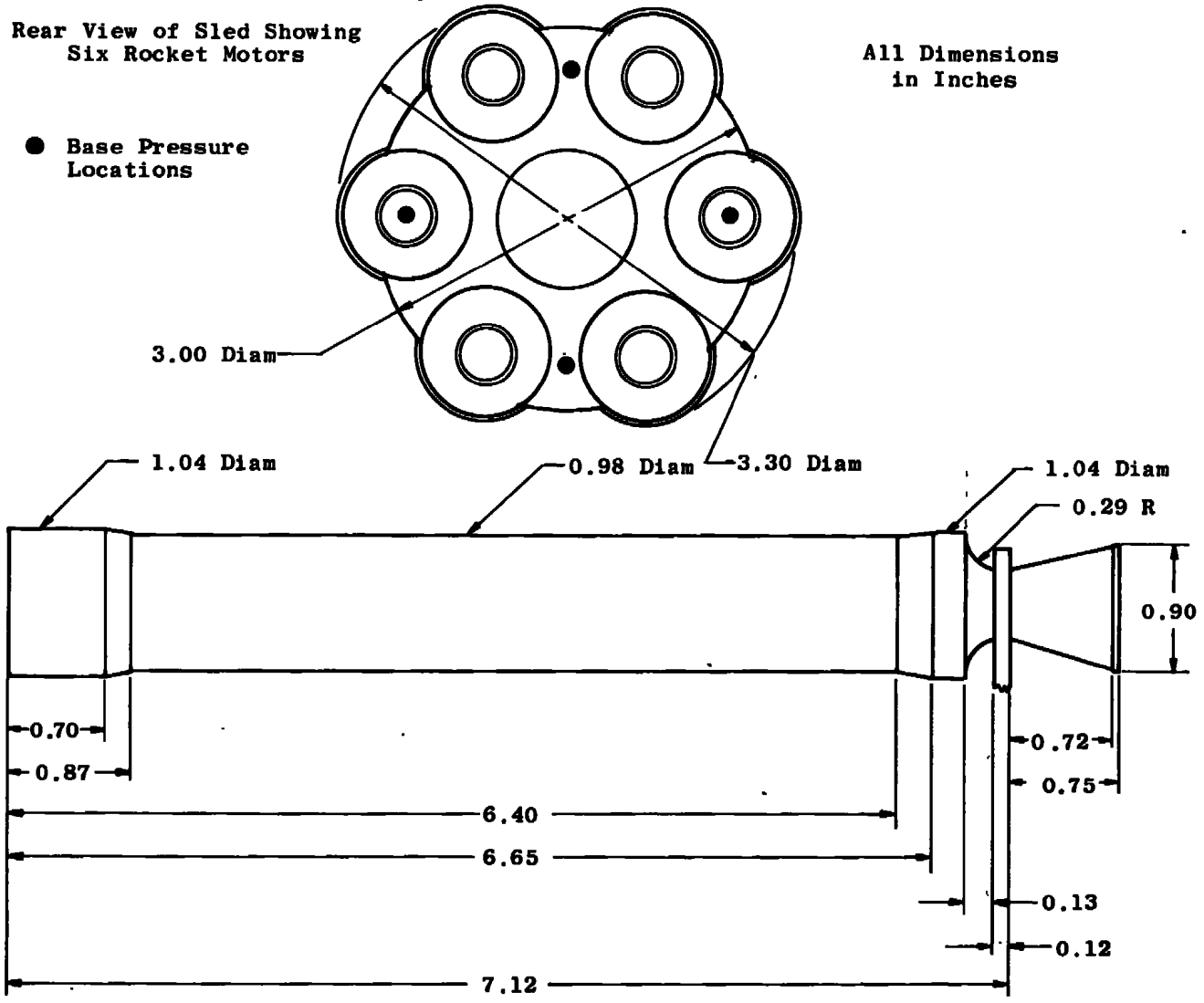
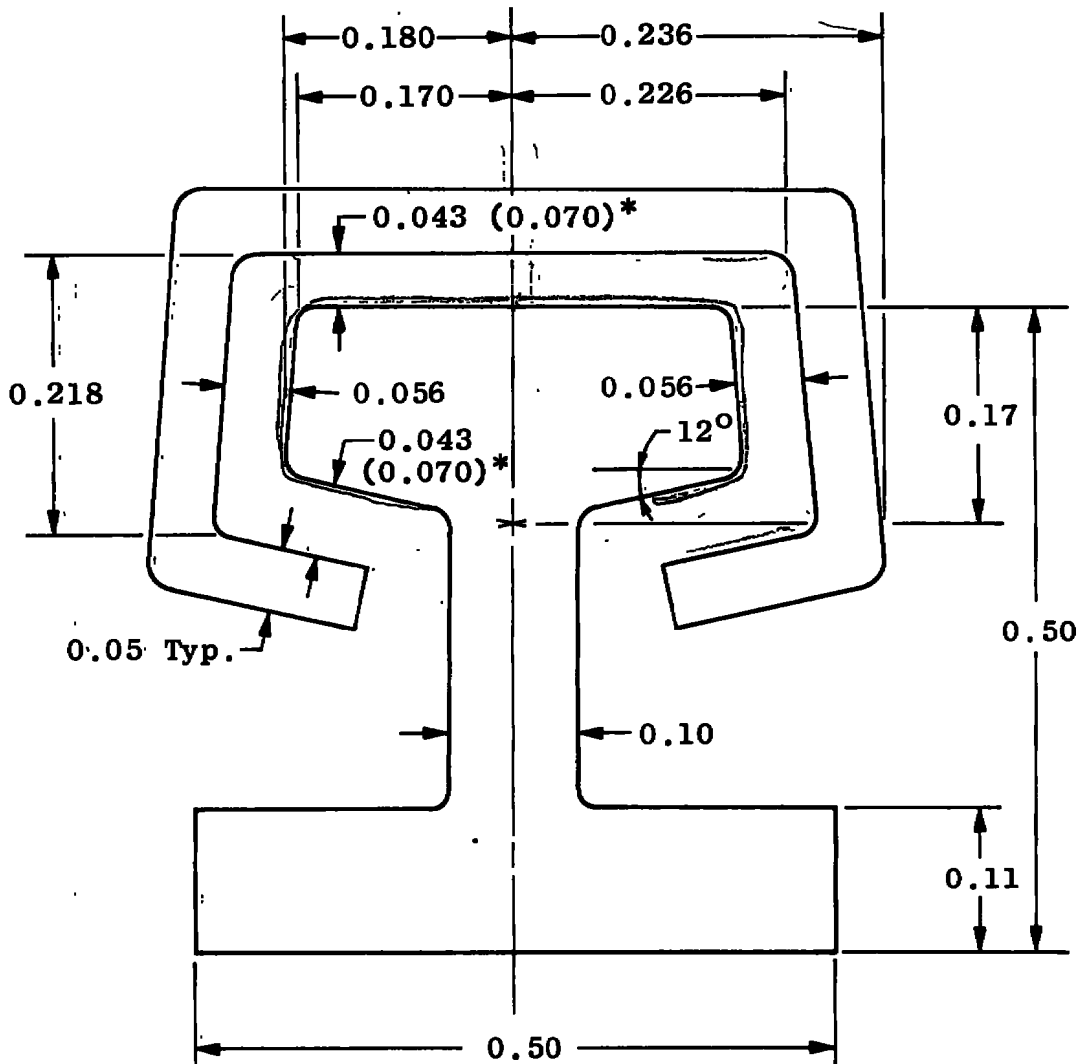


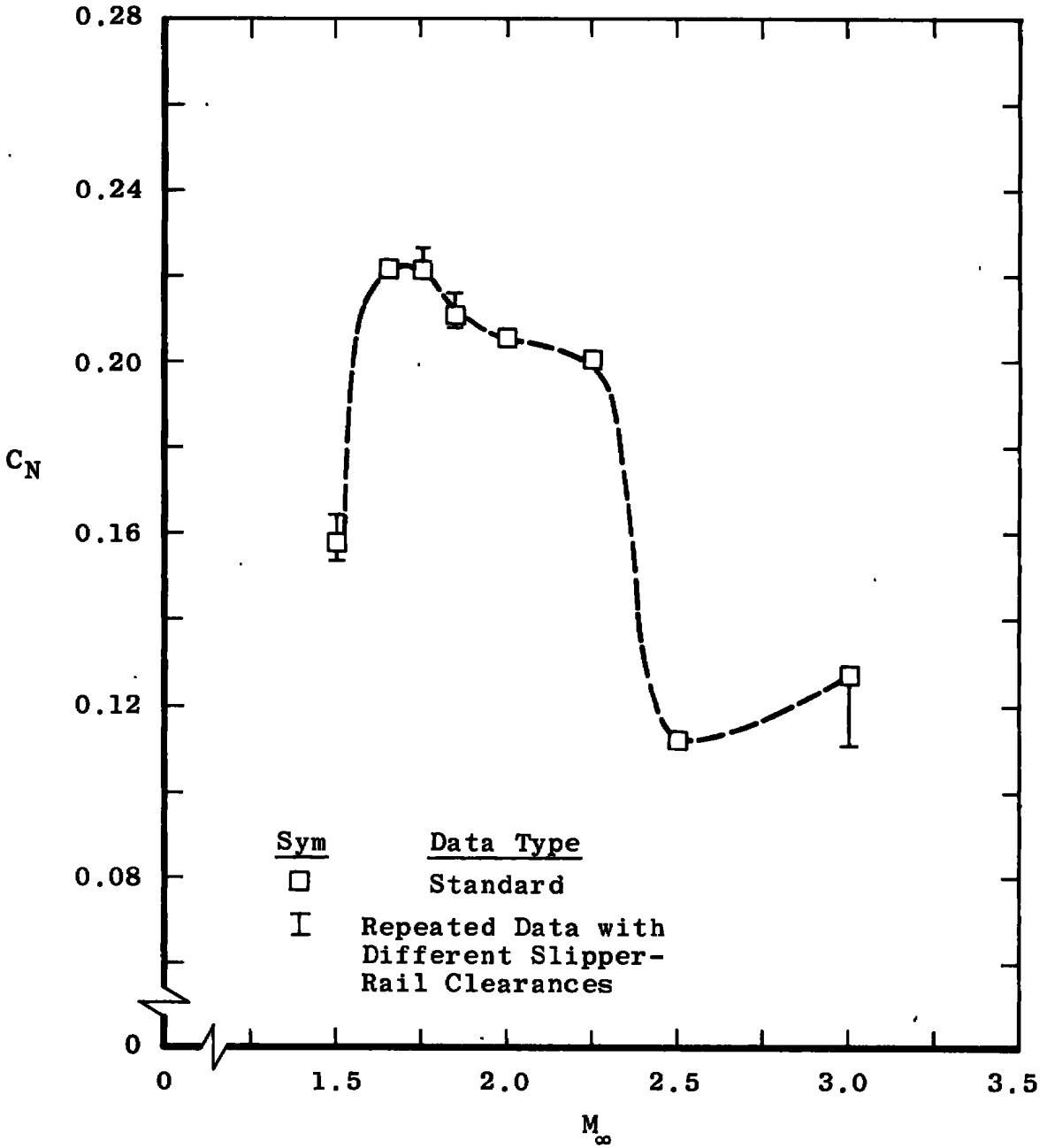
Figure 6. Rocket motor details.



*Actual dimensions are shown
in the parentheses.

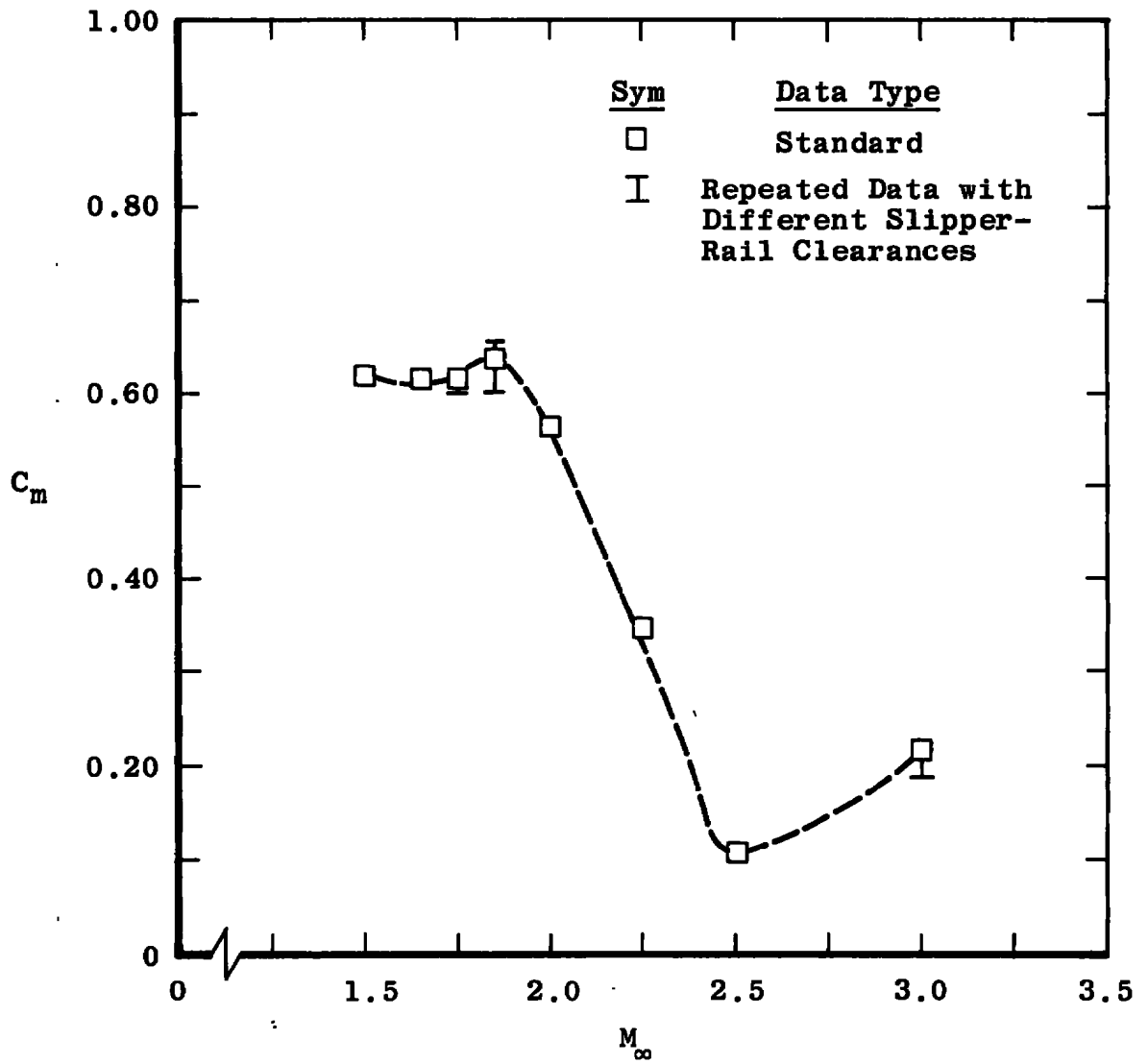
All Dimensions
in Inches

Figure 7. Typical slipper and rail cross section.

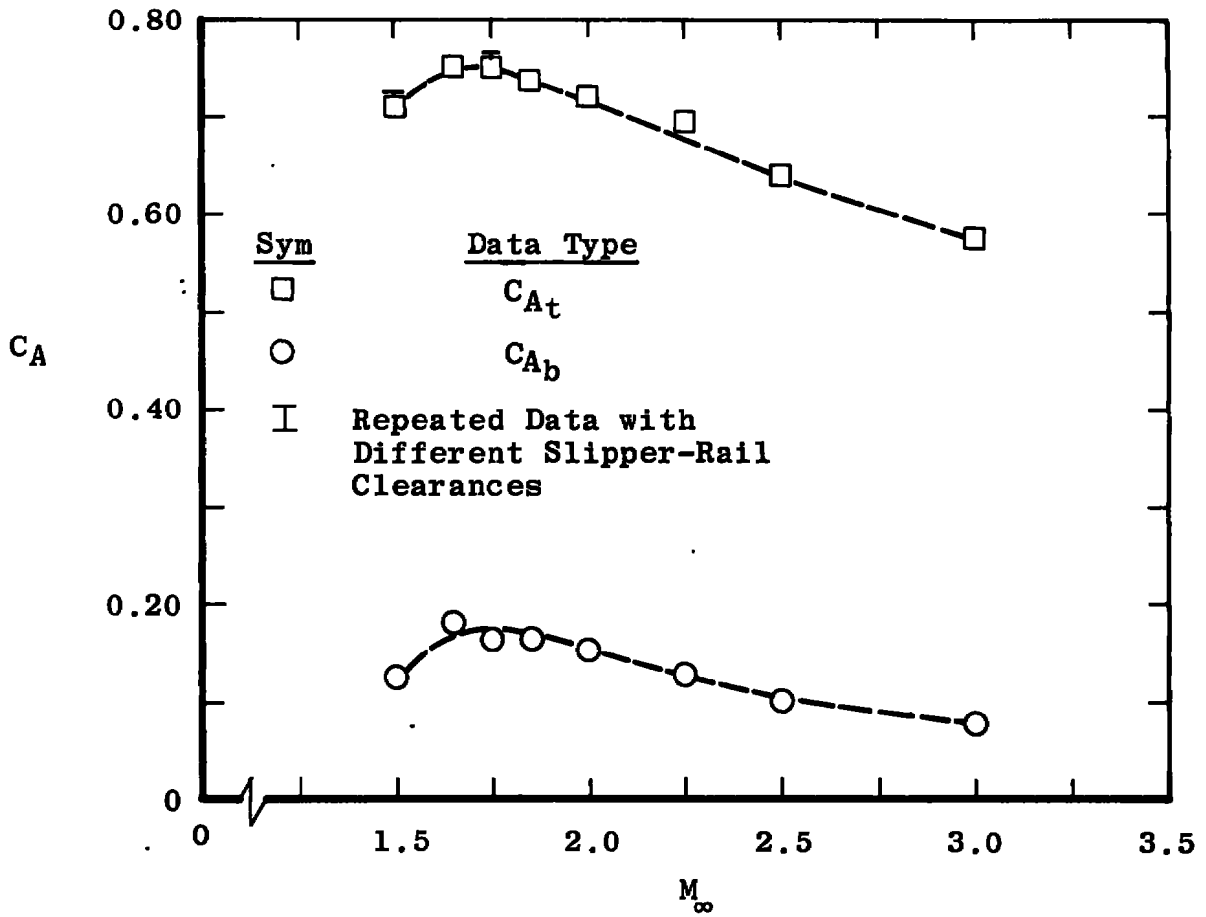


a. C_N versus M_∞

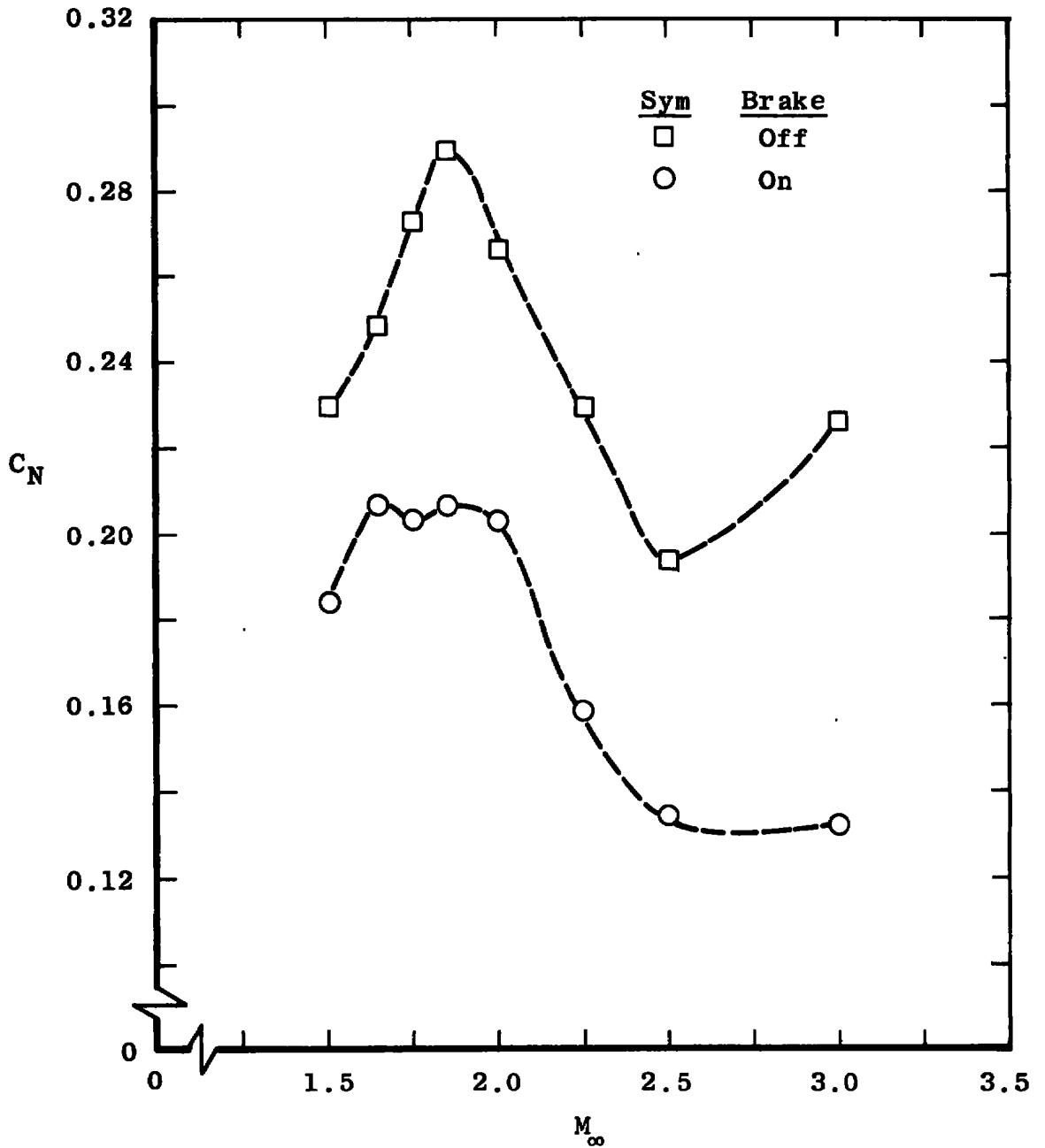
Figure 8. Typical effects of a change in slipper to rail clearance (configuration 2.2.1.2.1).



b. C_m versus M_∞
Figure 8. Continued.

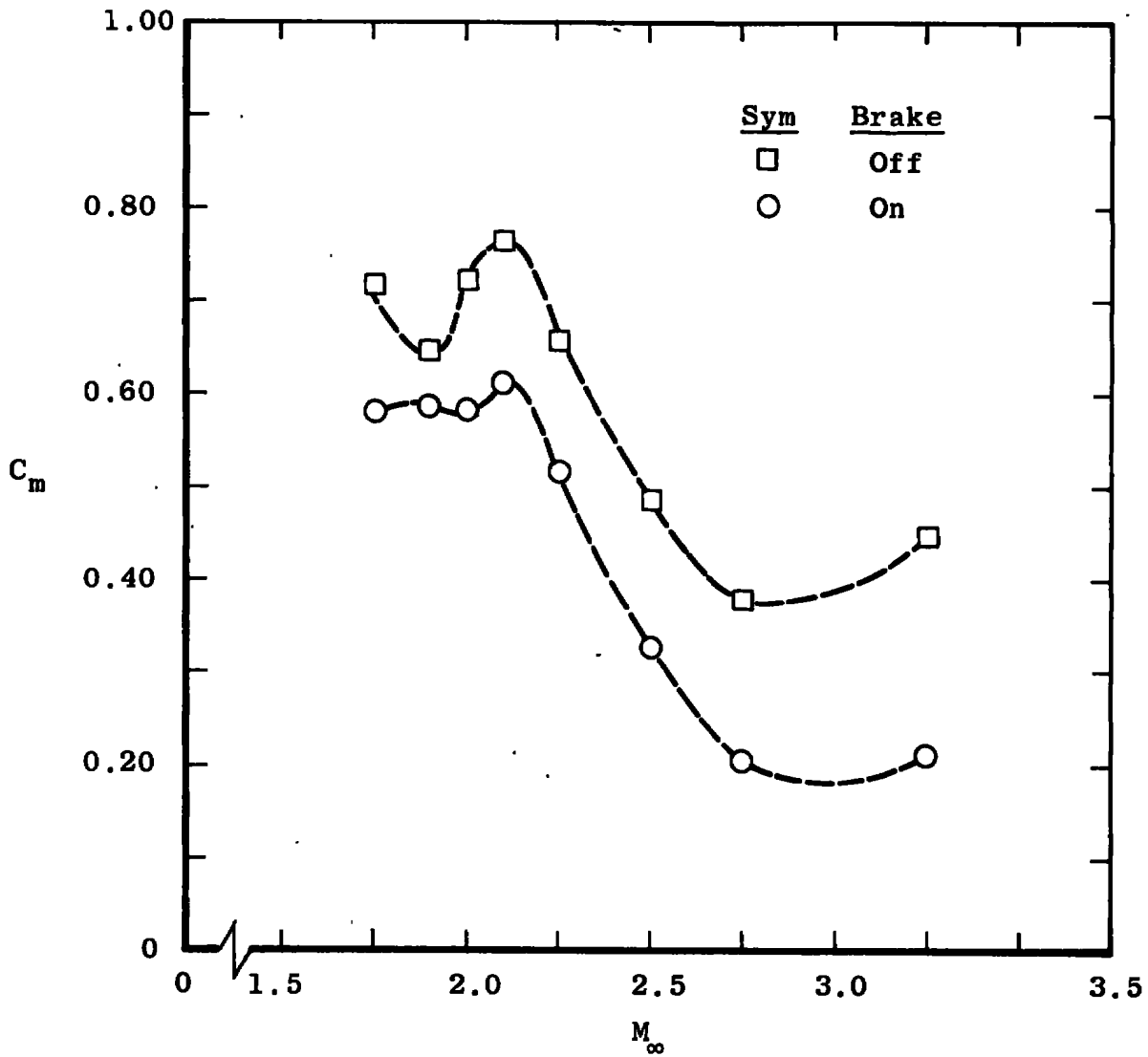


c. C_A versus M_∞
 Figure 8. Concluded.

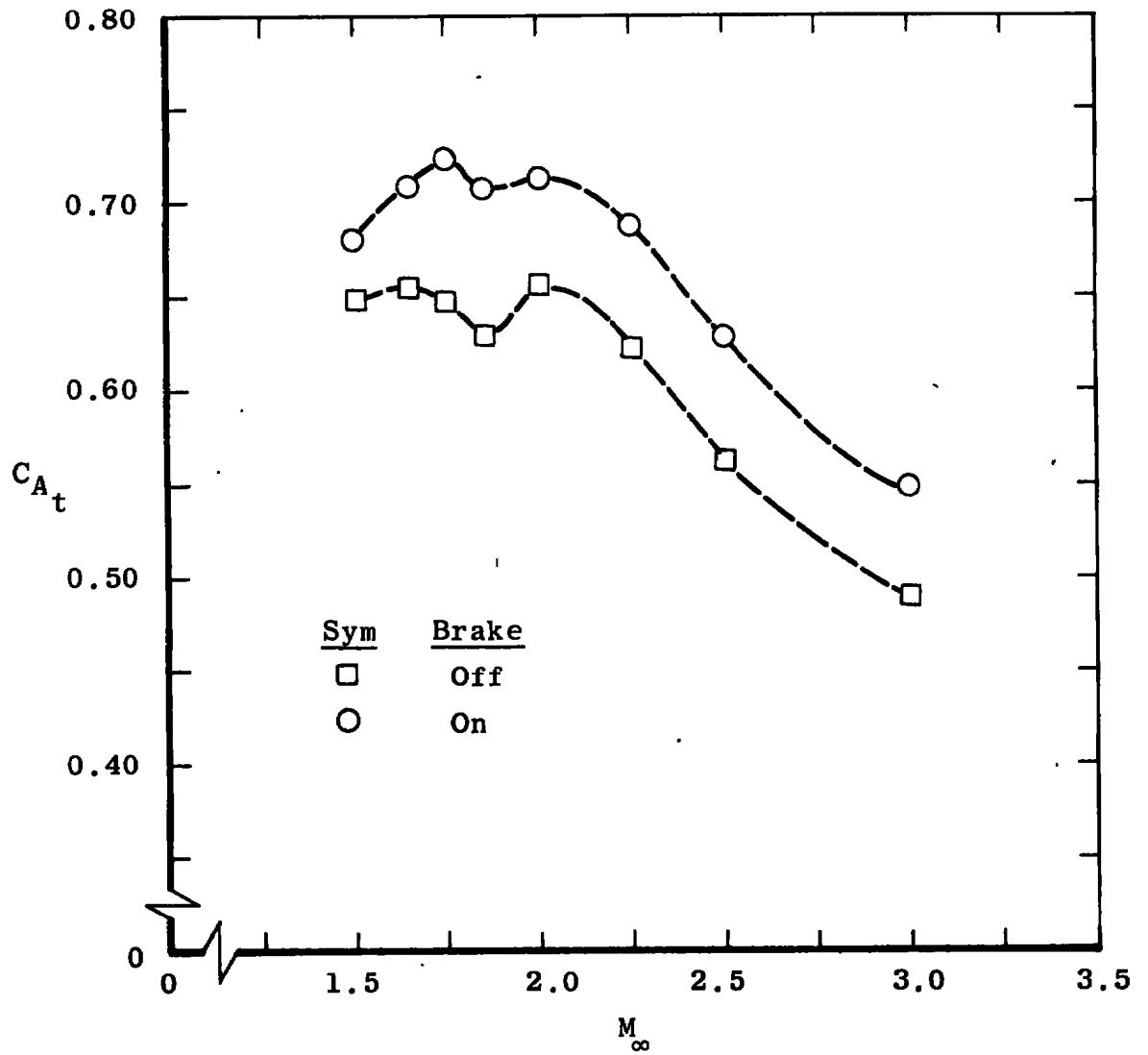


a. C_N versus M_∞

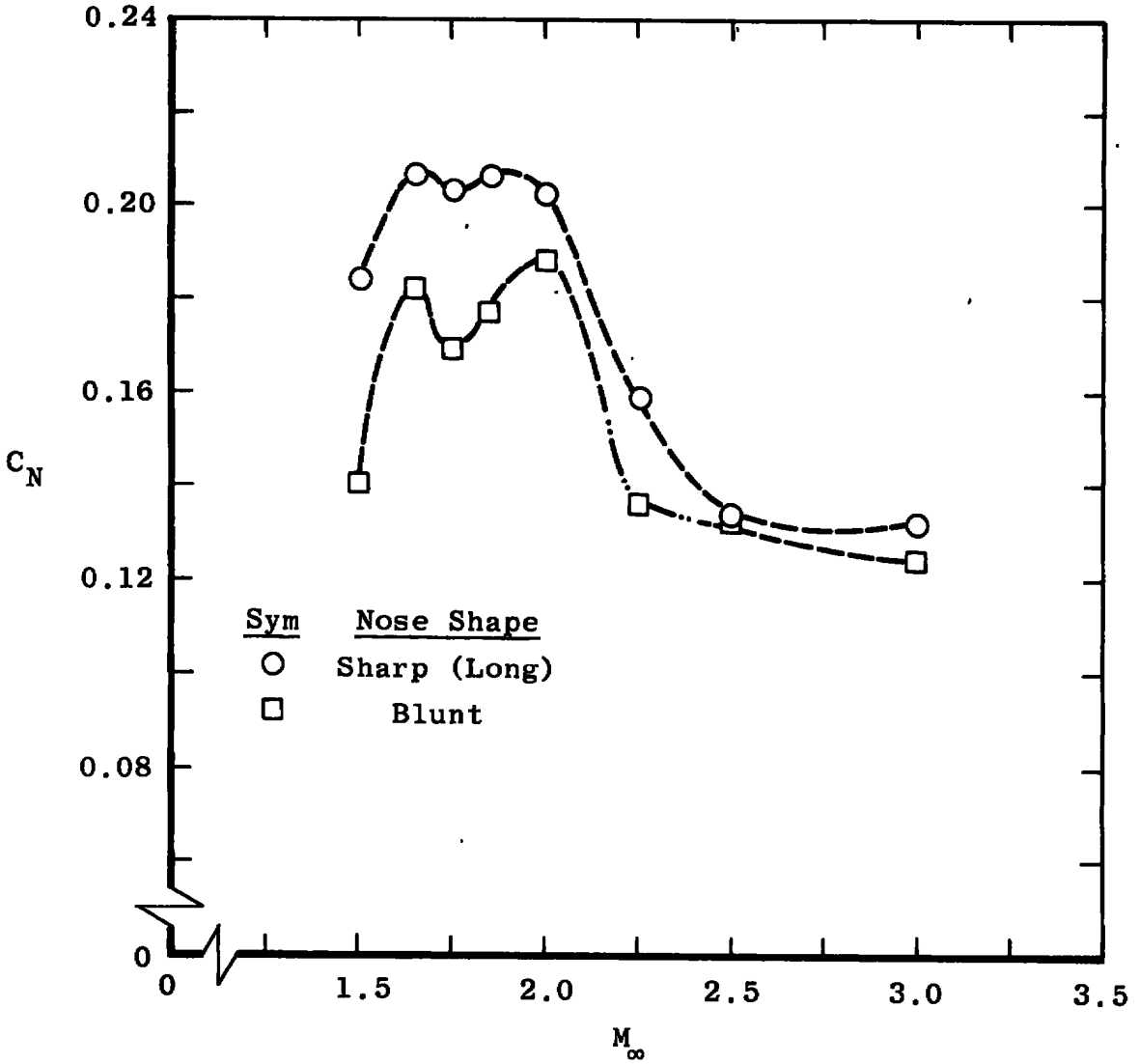
Figure 9. Effect of water brake on long cone configuration with short slippers in the forward position (1.3.1.2.X).



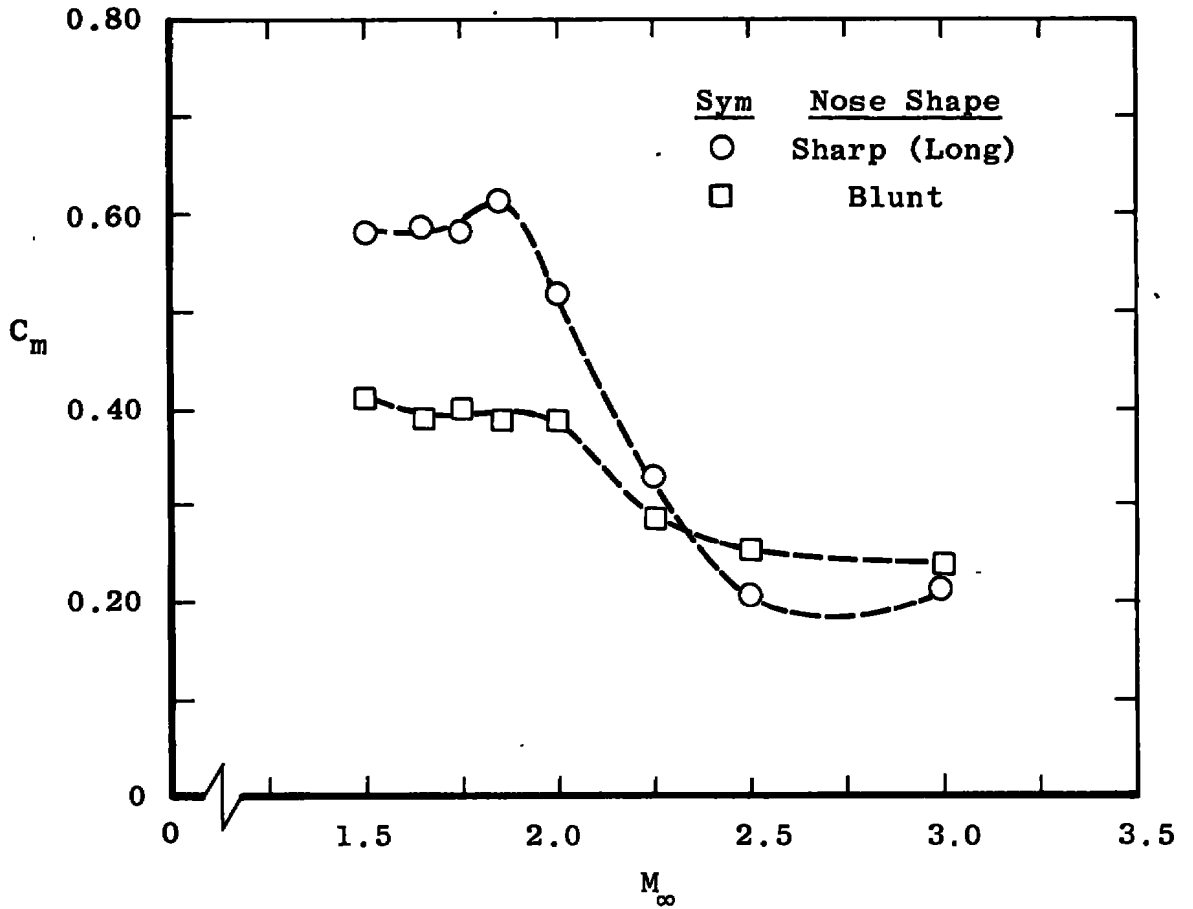
b. C_m versus M_∞
 Figure 9. Continued.



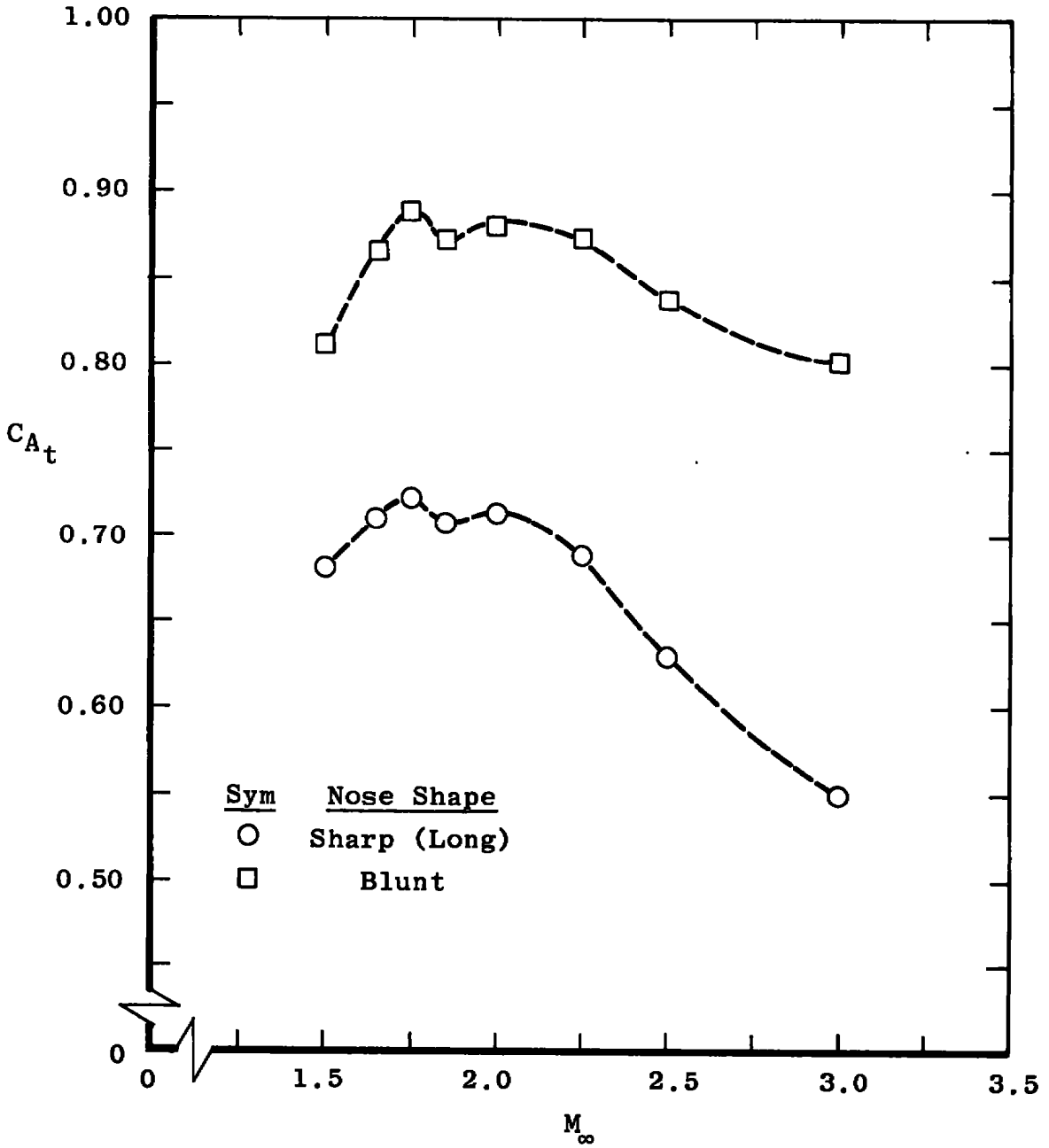
c. C_{A_t} versus M_∞
Figure 9. Concluded.



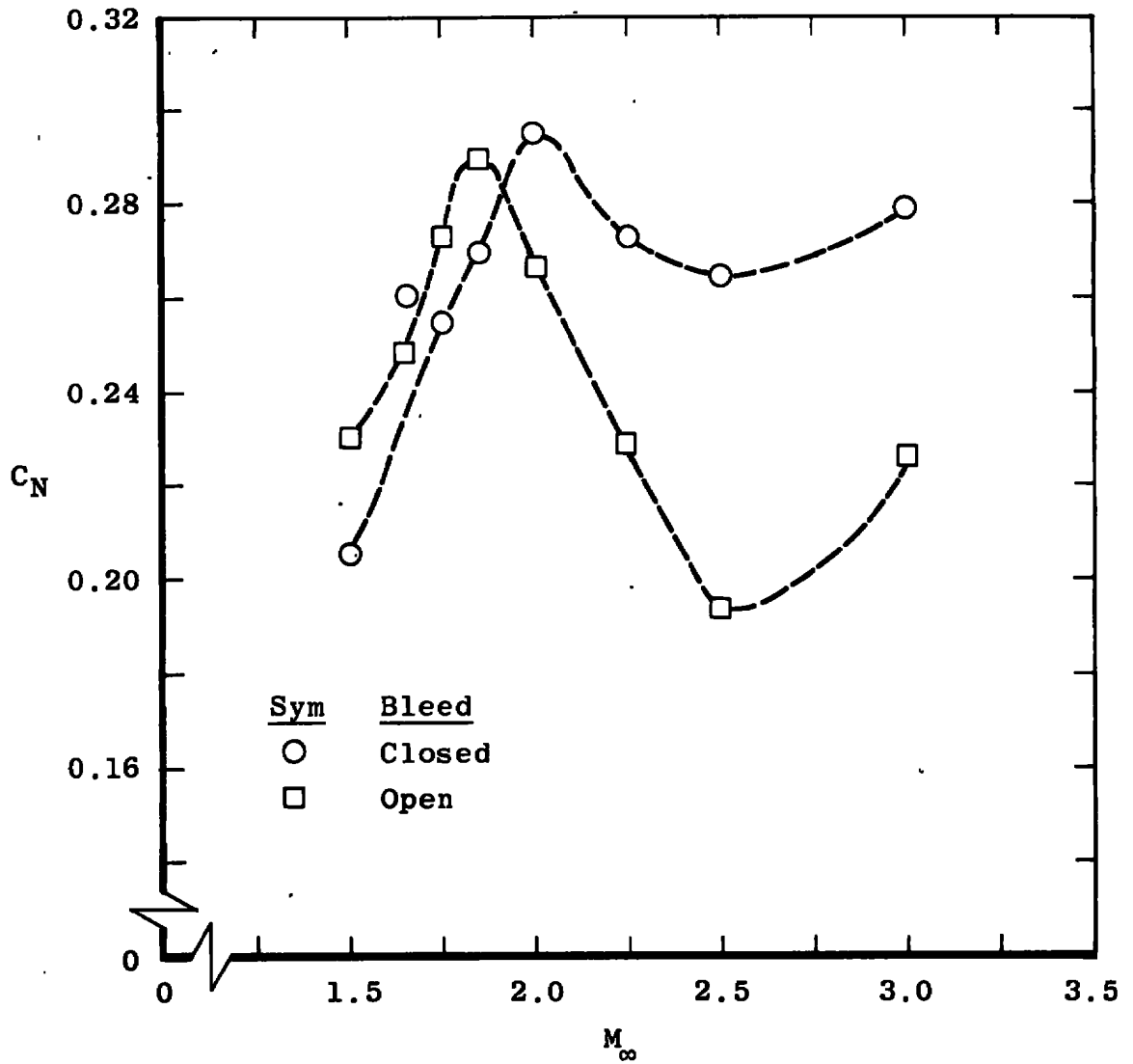
a. C_N versus M_∞
 Figure 10. Effect of nose shape with the short slippers in the forward position (1.3.1.X.1).



b. C_m versus M_∞
Figure 10. Continued.

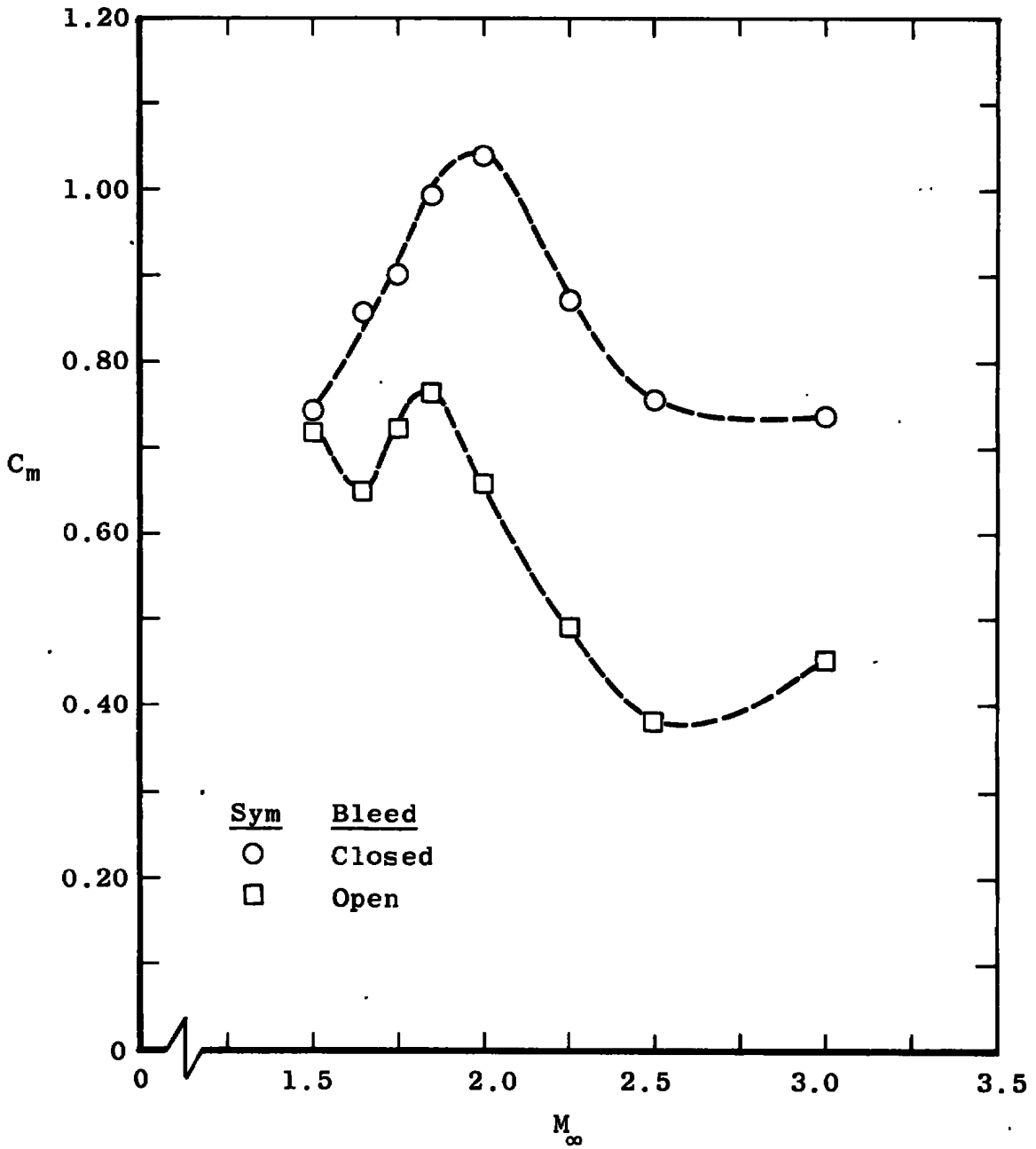


c. C_{A_t} versus M_∞
 Figure 10. Concluded.

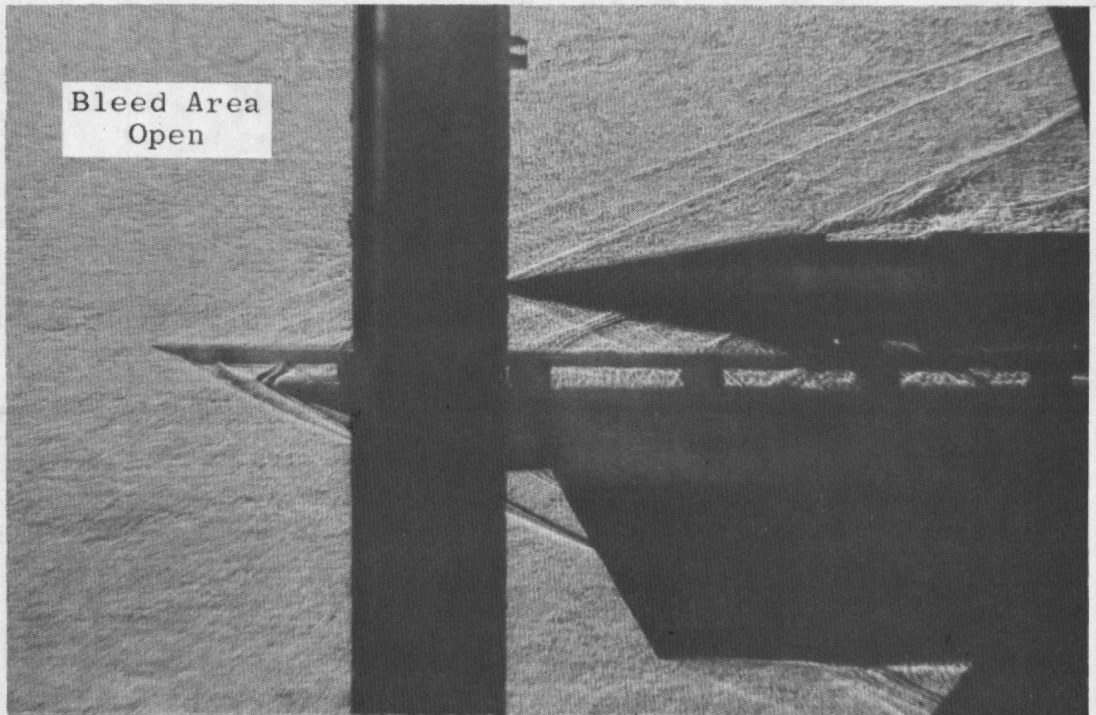
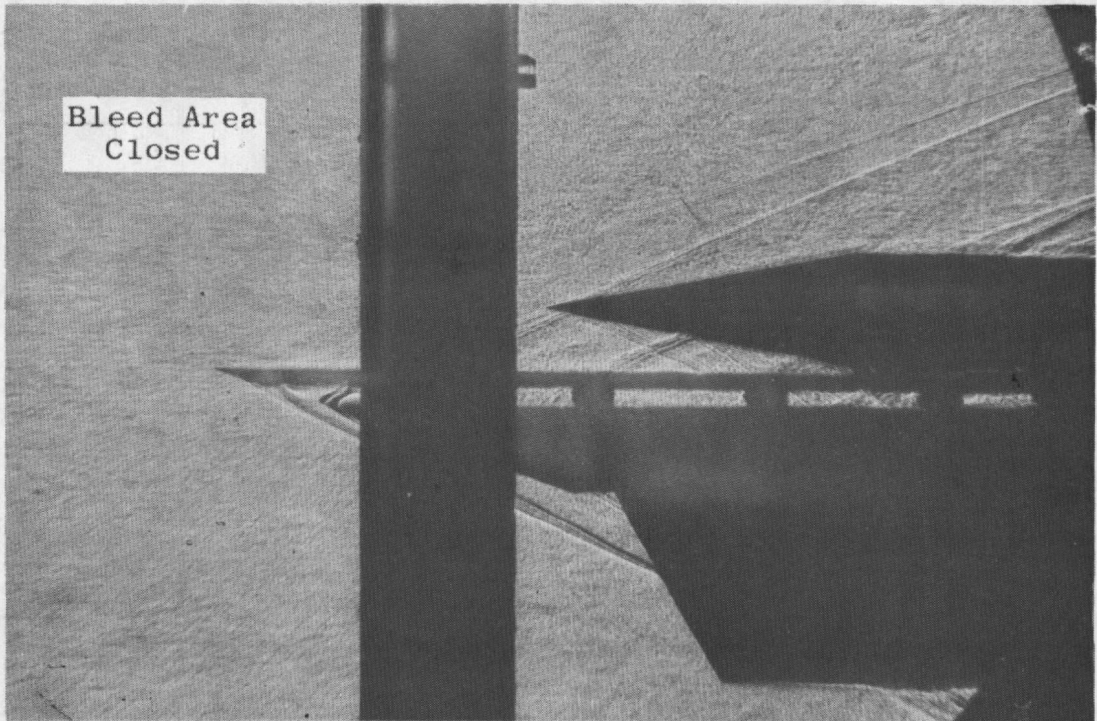


a. C_N versus M_∞

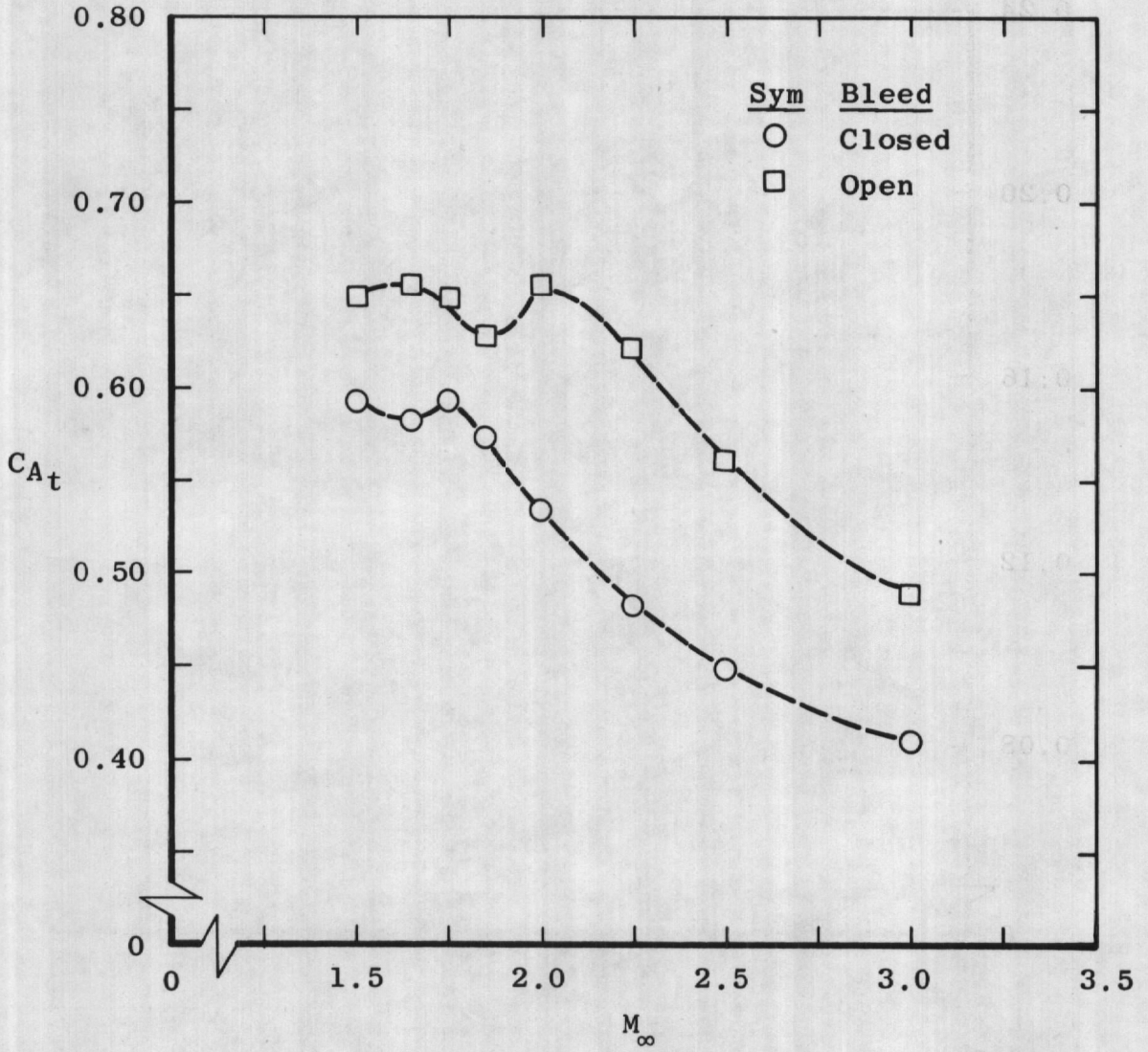
Figure 11. Effect of bleed opening on long cone configuration with short slippers in the forward position (1.3.X.2.2).



b. C_m versus M_∞
 Figure 11. Continued.



c. Shadowgraphs showing bleed effect, $M_\infty = 3.0$
Figure 11. Continued.



d. C_{A_t} versus M_∞
 Figure 11. Concluded.

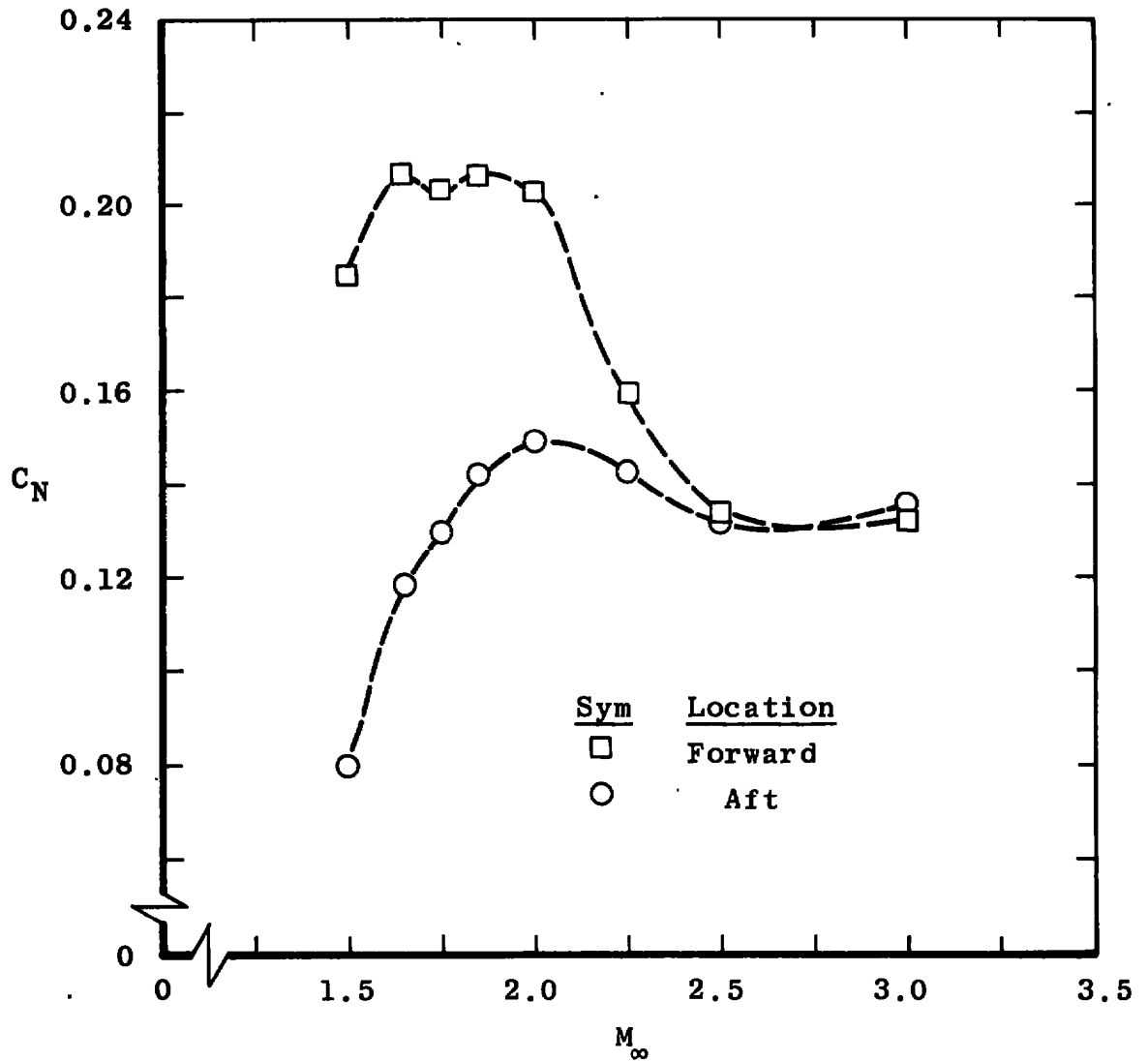
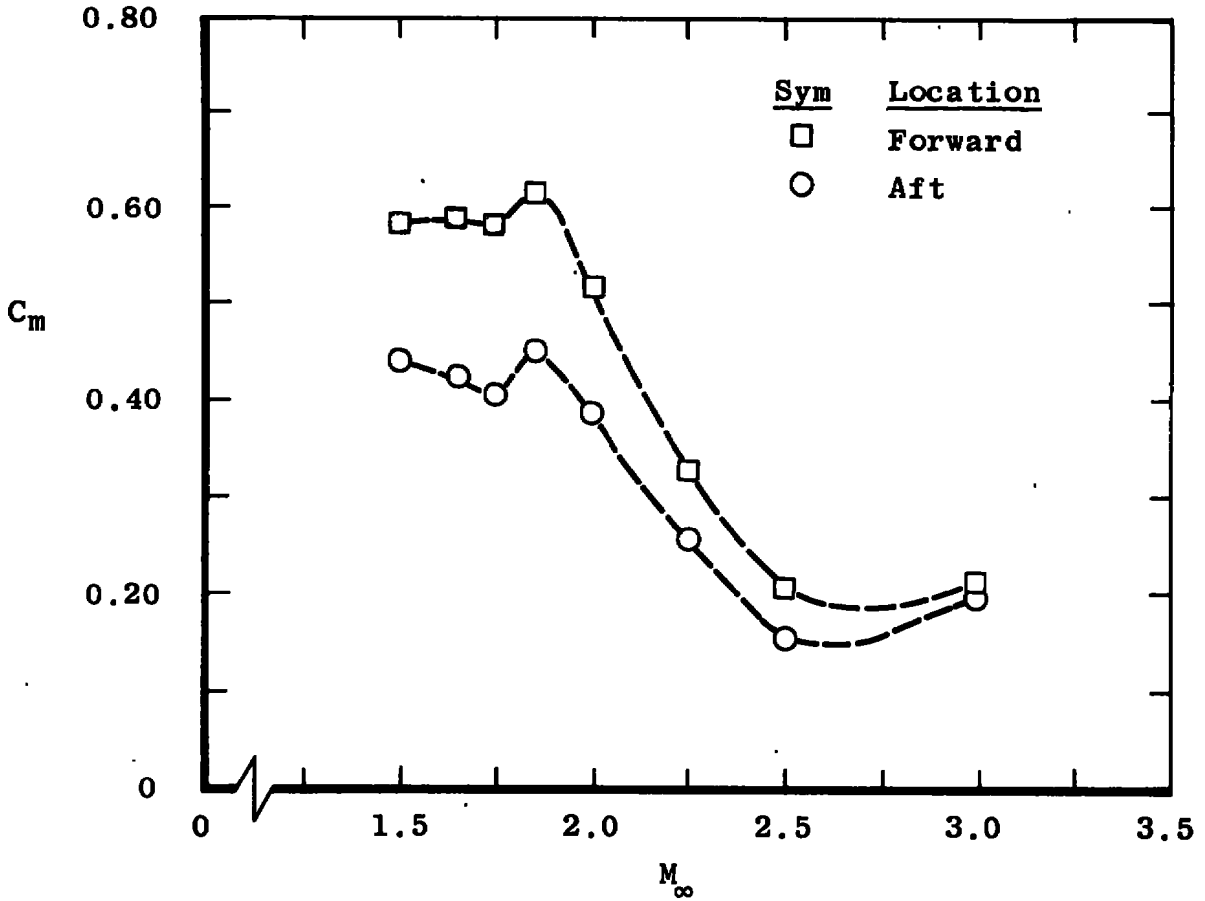
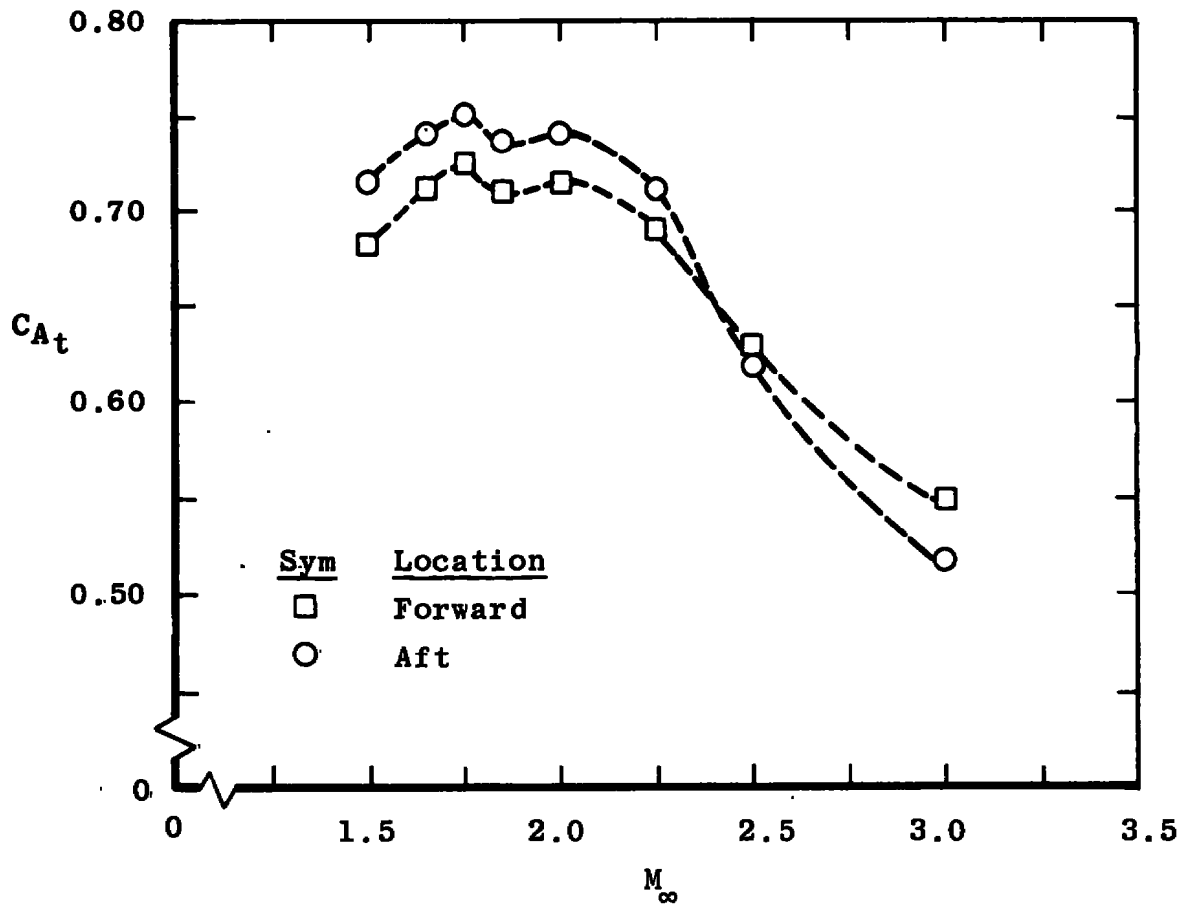
a. C_N versus M_∞

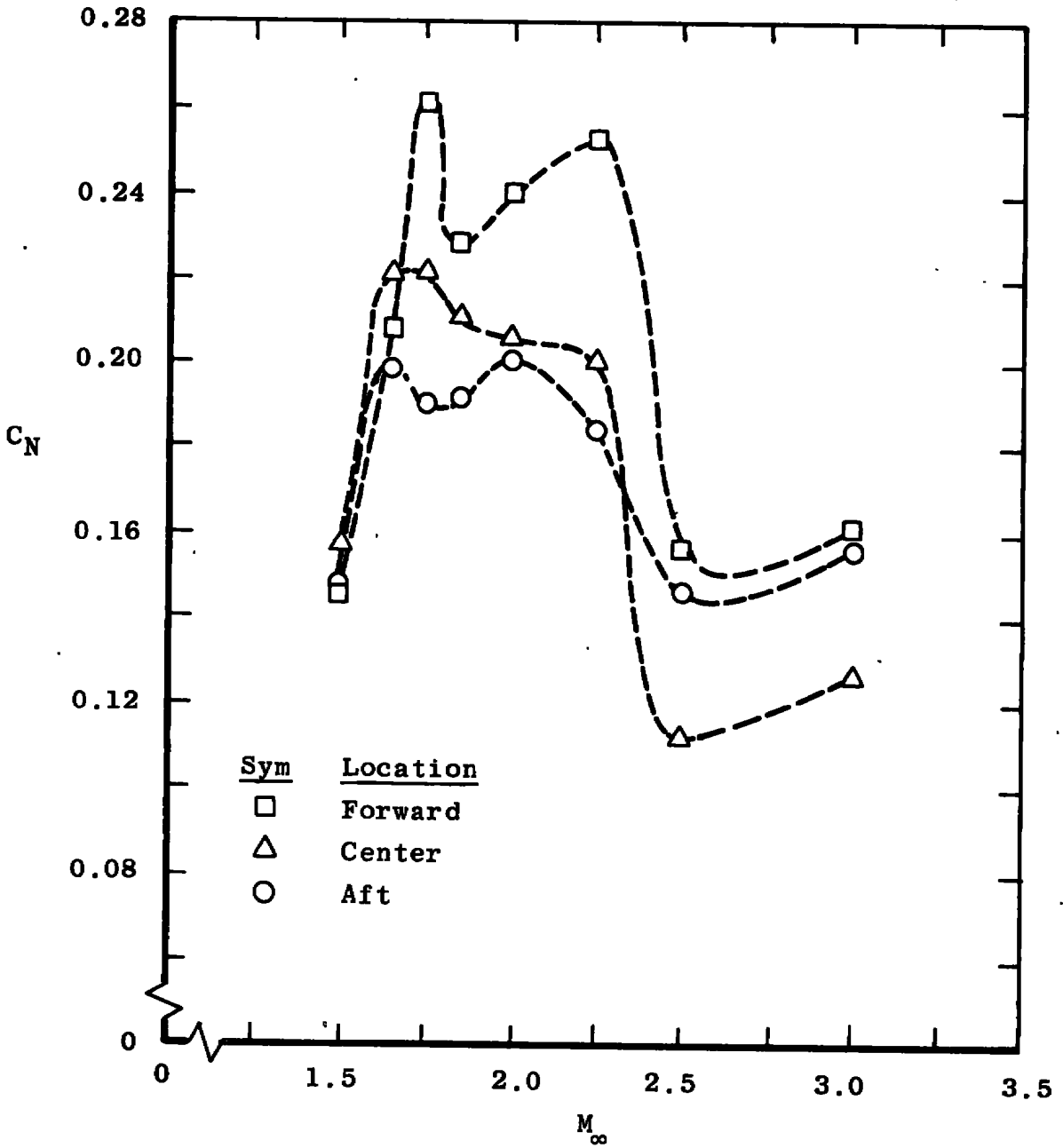
Figure 12. Effect of short slipper locations on the long cone (1.X.1.2.1).



b. C_m versus M_∞
 Figure 12. Continued.

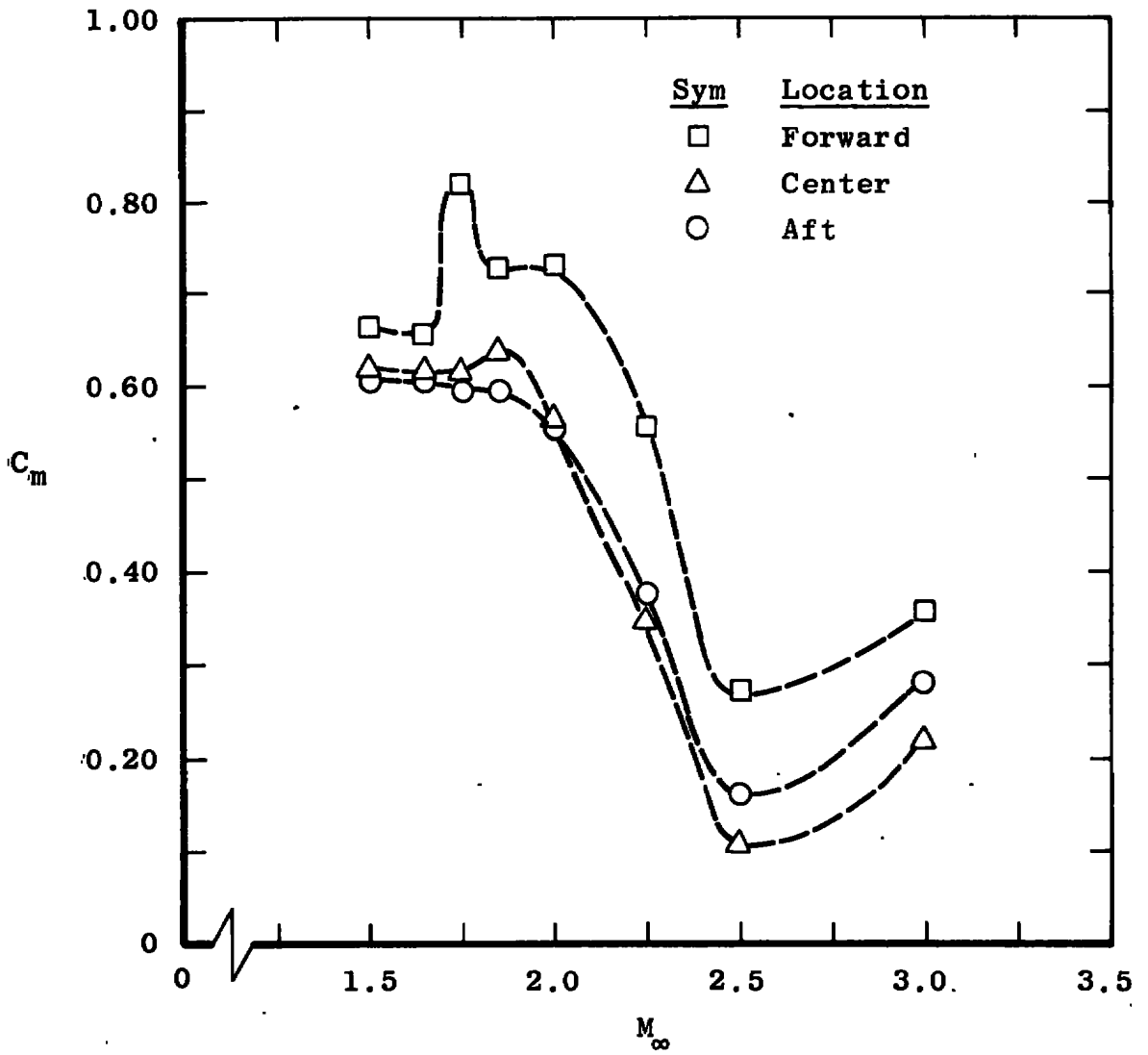


c. C_{At} versus M_∞
Figure 12. Concluded.

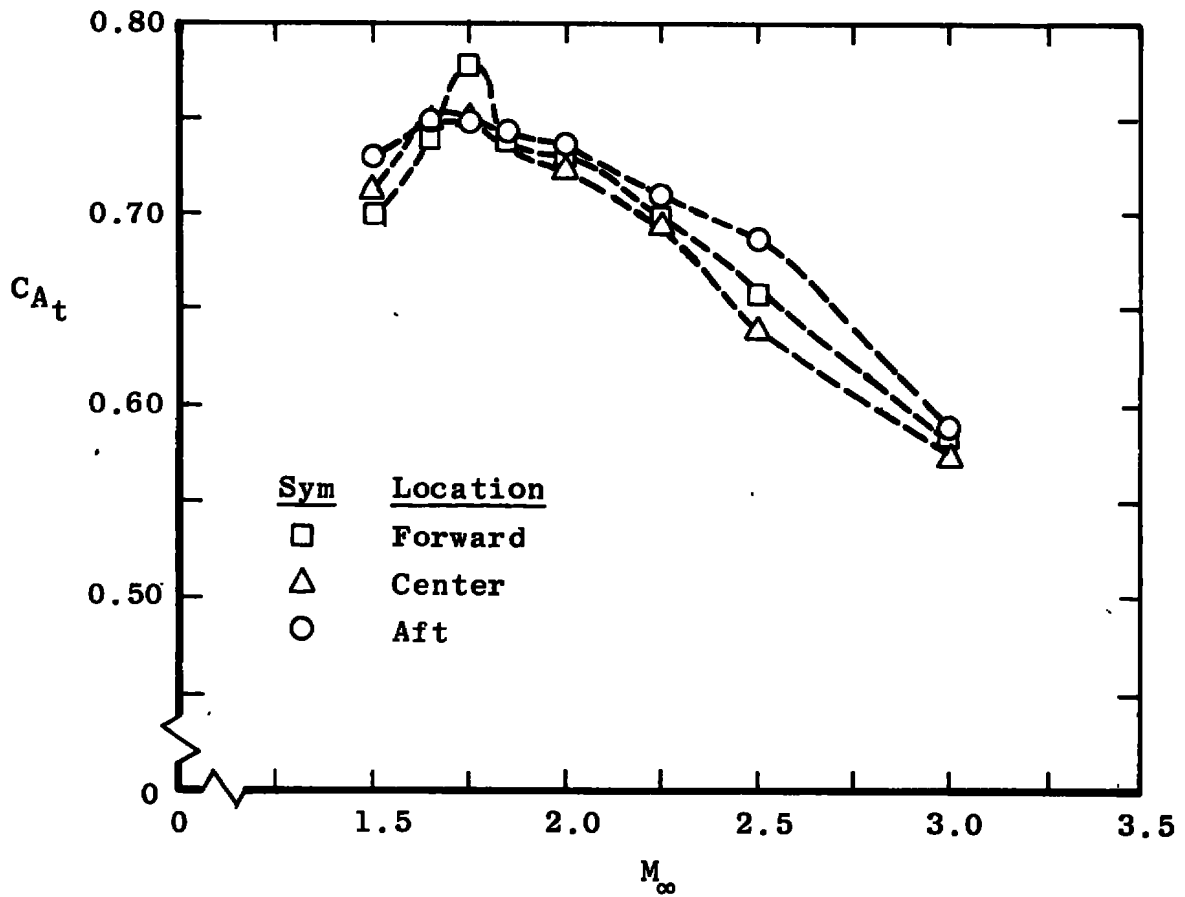


a. C_N versus M_∞

Figure 13. Effect of medium slipper locations on the long cone (2.X.1.2.1).



b. C_m versus M_∞
Figure 13. Continued.



c. C_{A_t} versus M_∞
 Figure 13. Concluded.

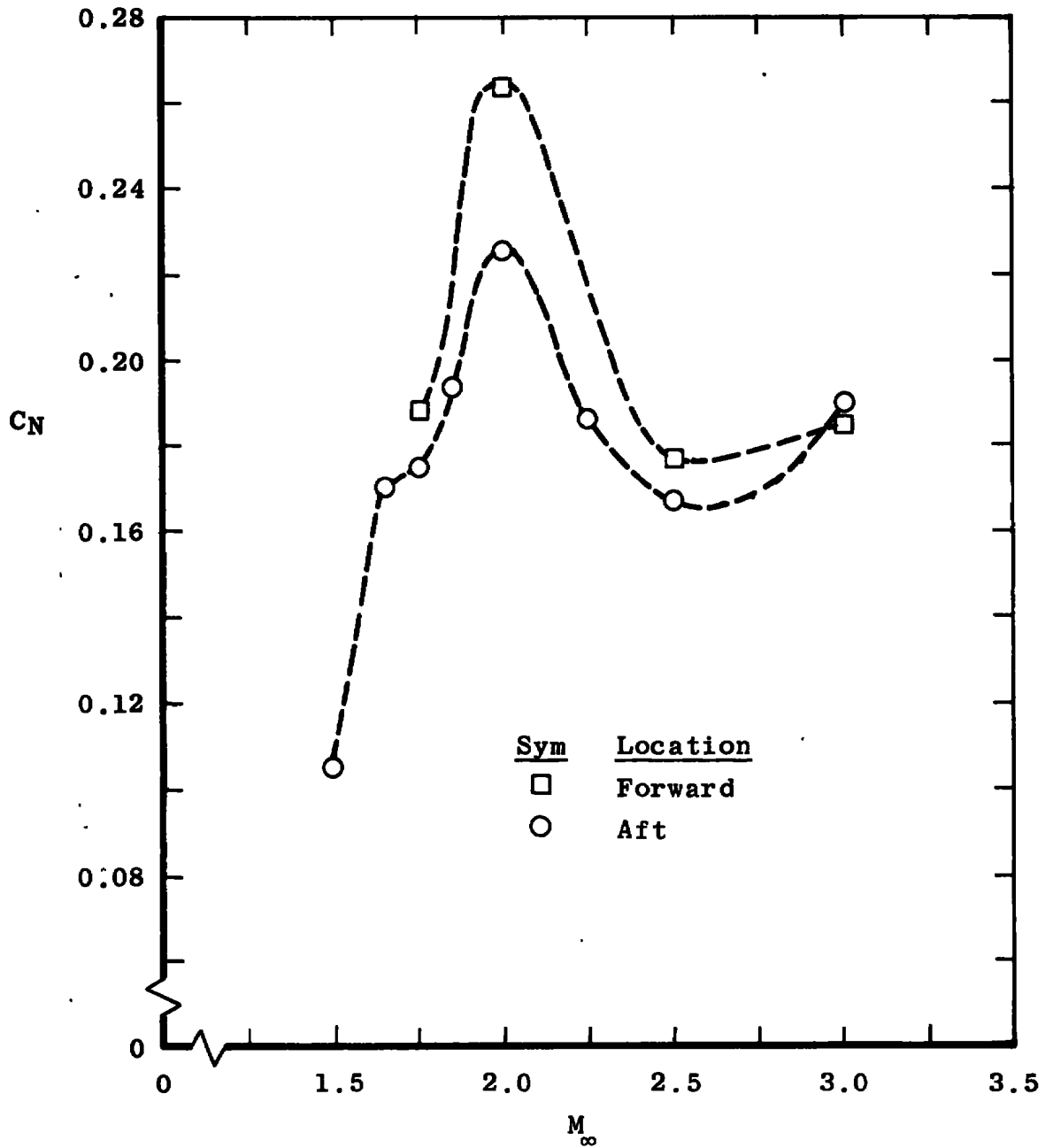
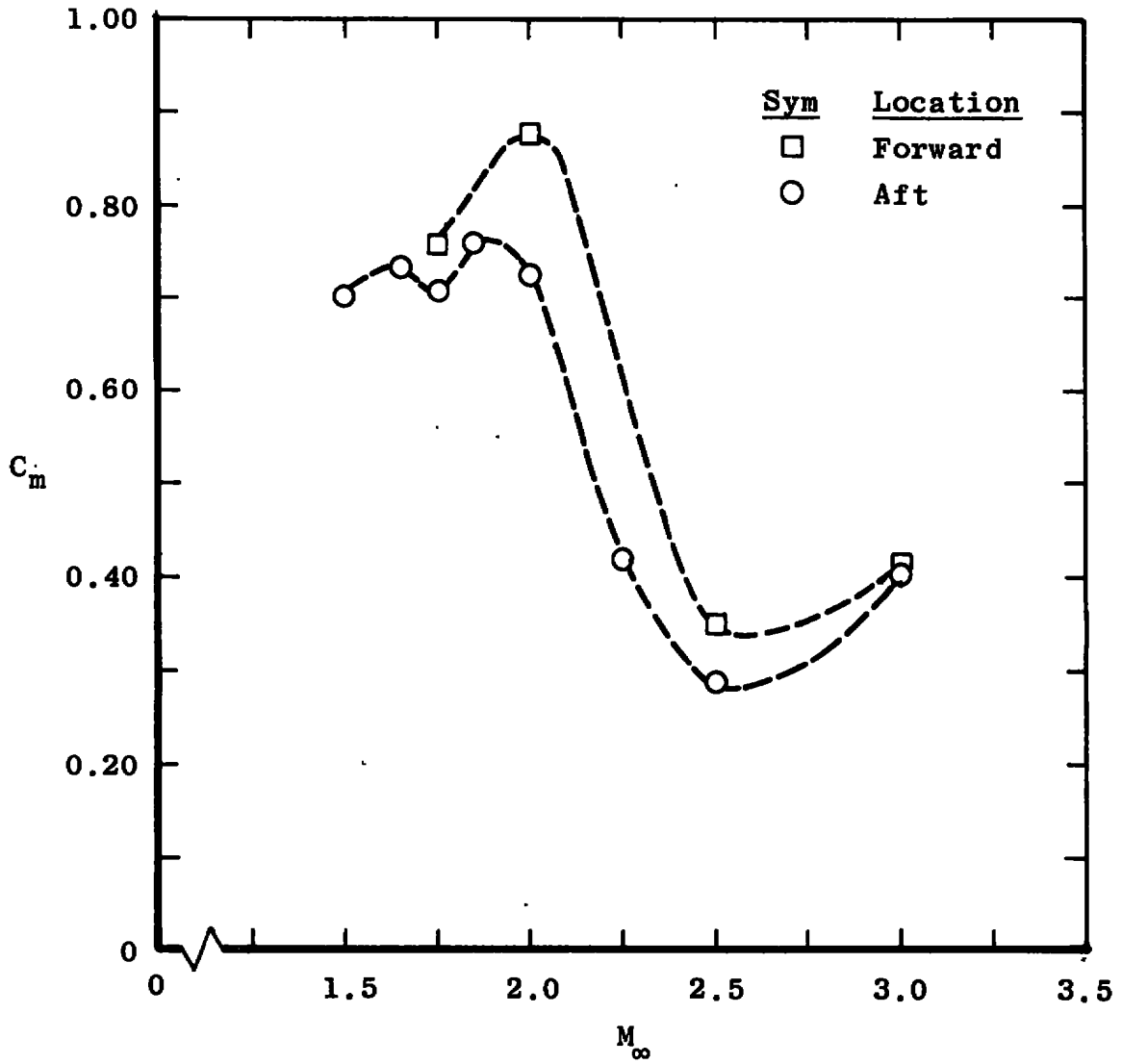
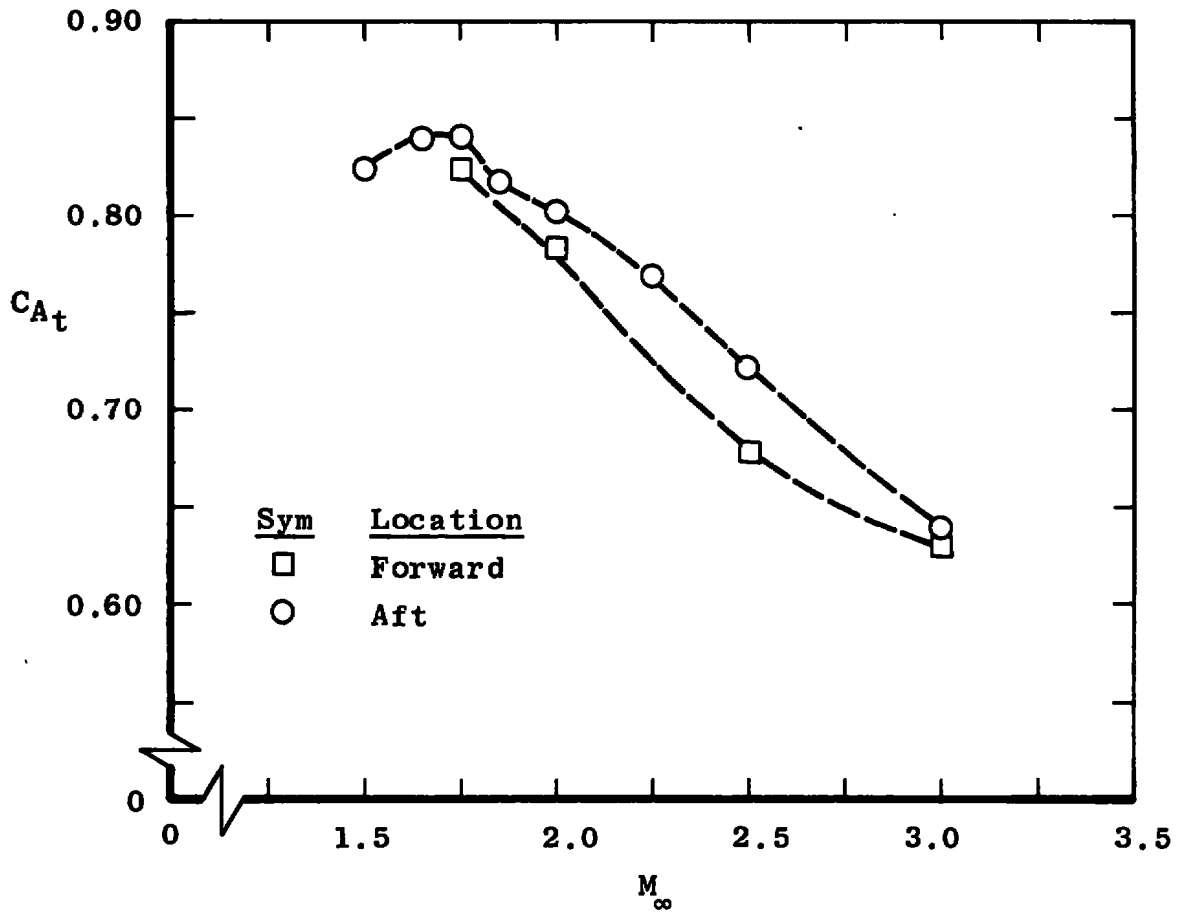
a. C_N versus M_∞

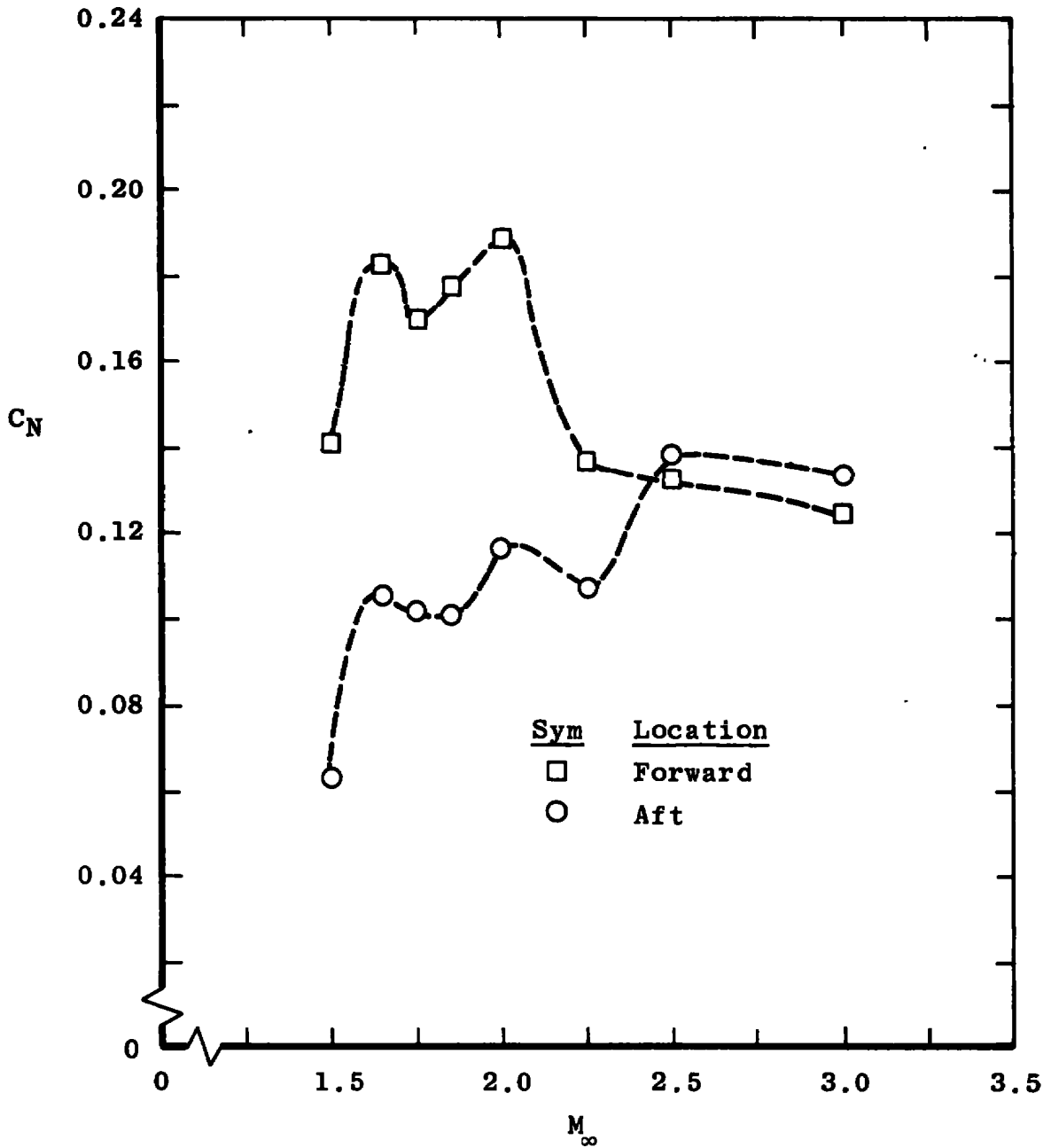
Figure 14. Effect of long slipper locations on the long cone (3.X.1.2.1).



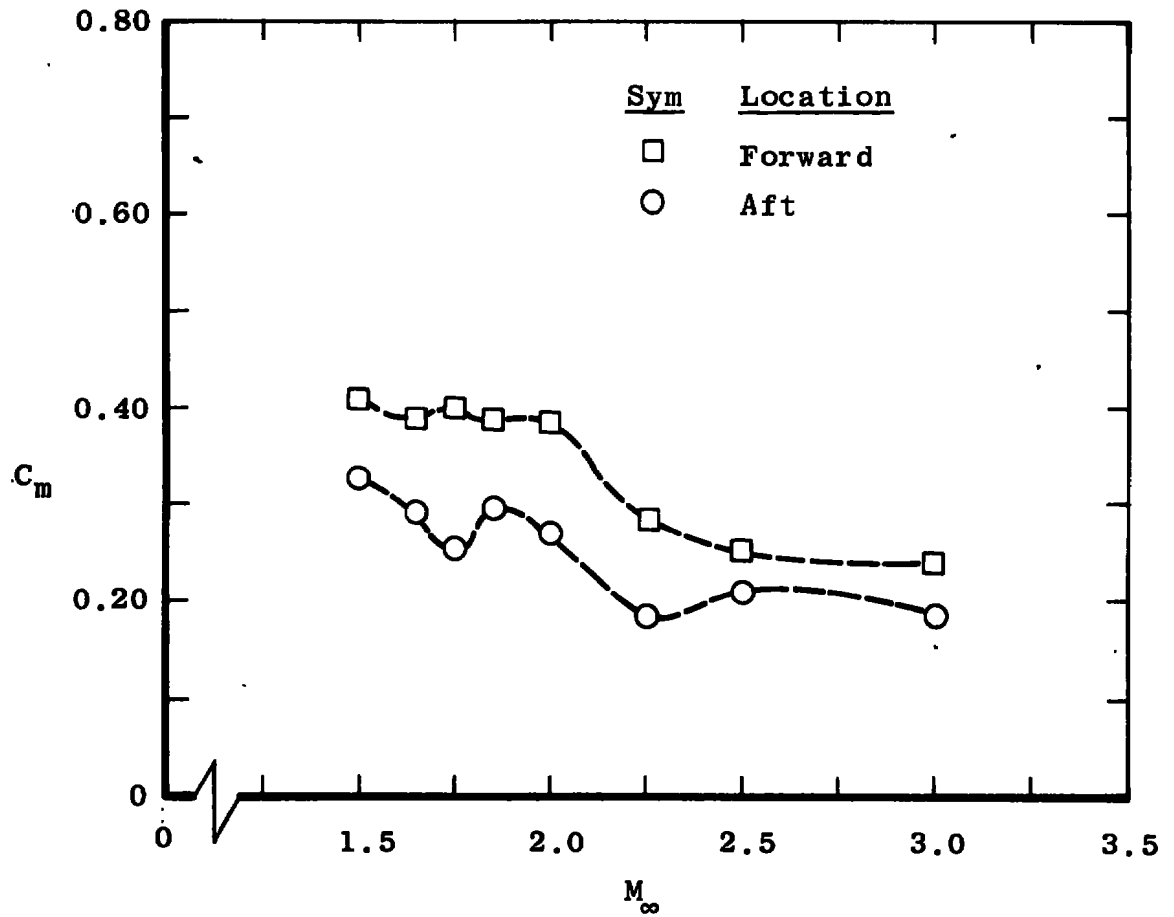
b. C_m versus M_∞
 Figure 14. Continued.



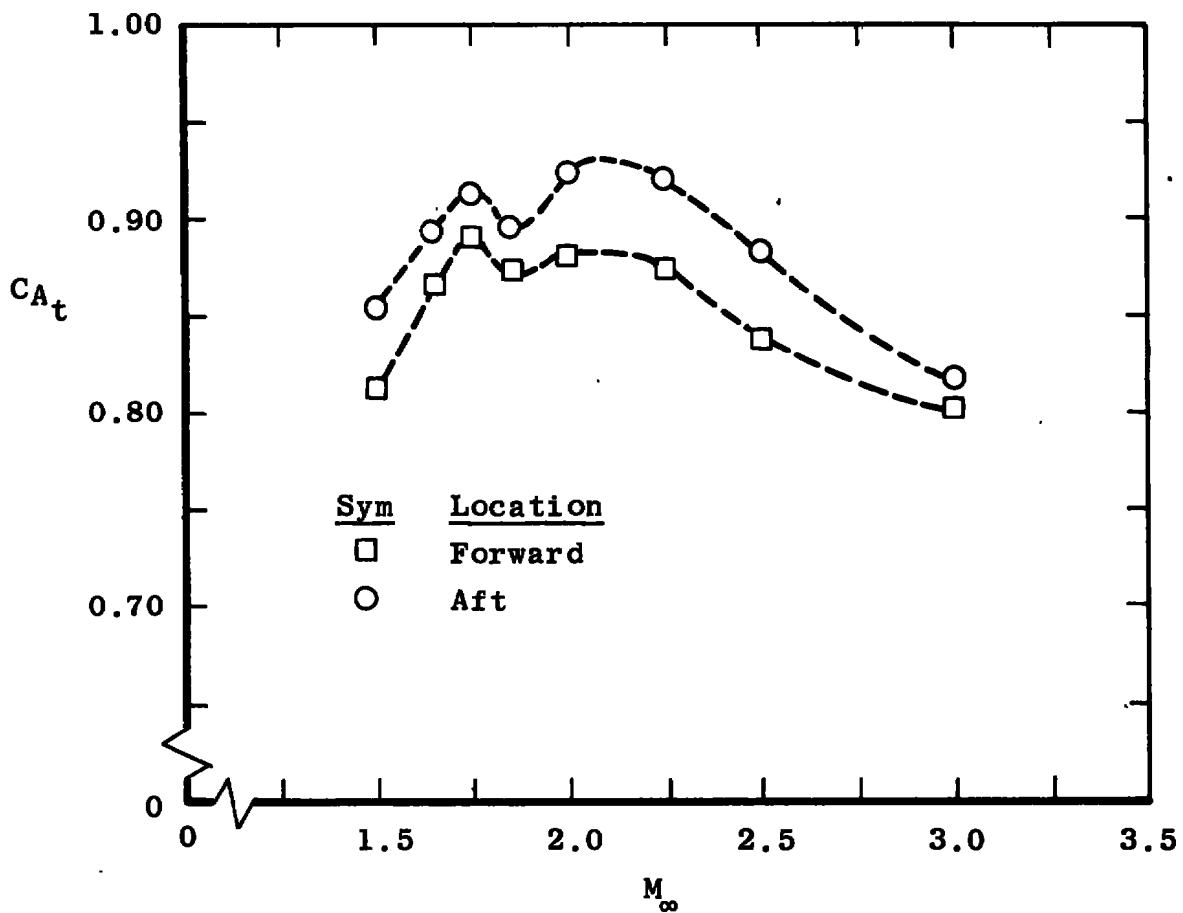
c. C_{A_t} versus M_∞
Figure 14. Concluded.



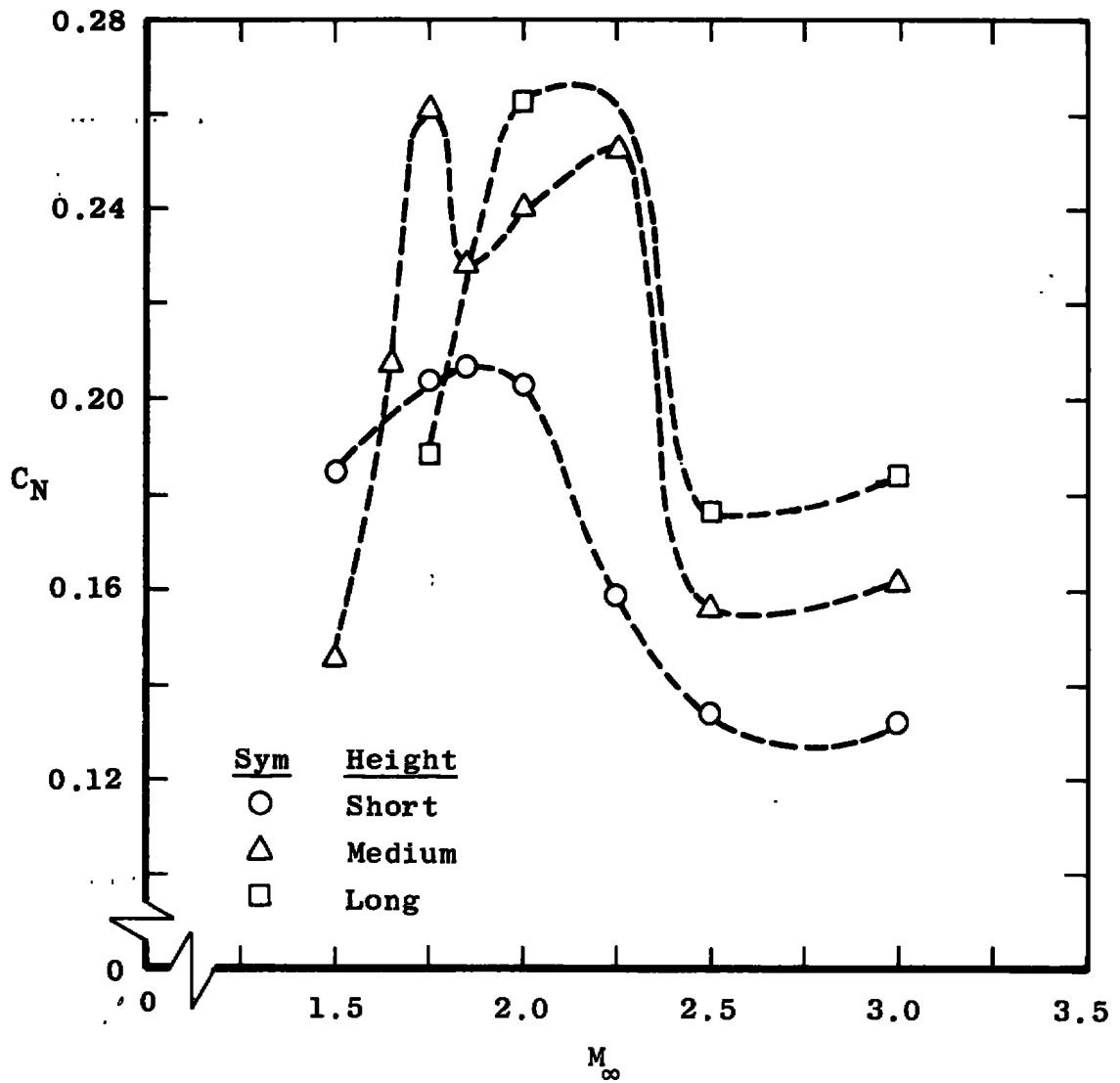
a. C_N versus M_∞
 Figure 15. Effect of short slipper locations on the blunt cone (1.X.1.3.1).



b. C_m versus M_∞
Figure 15. Continued.

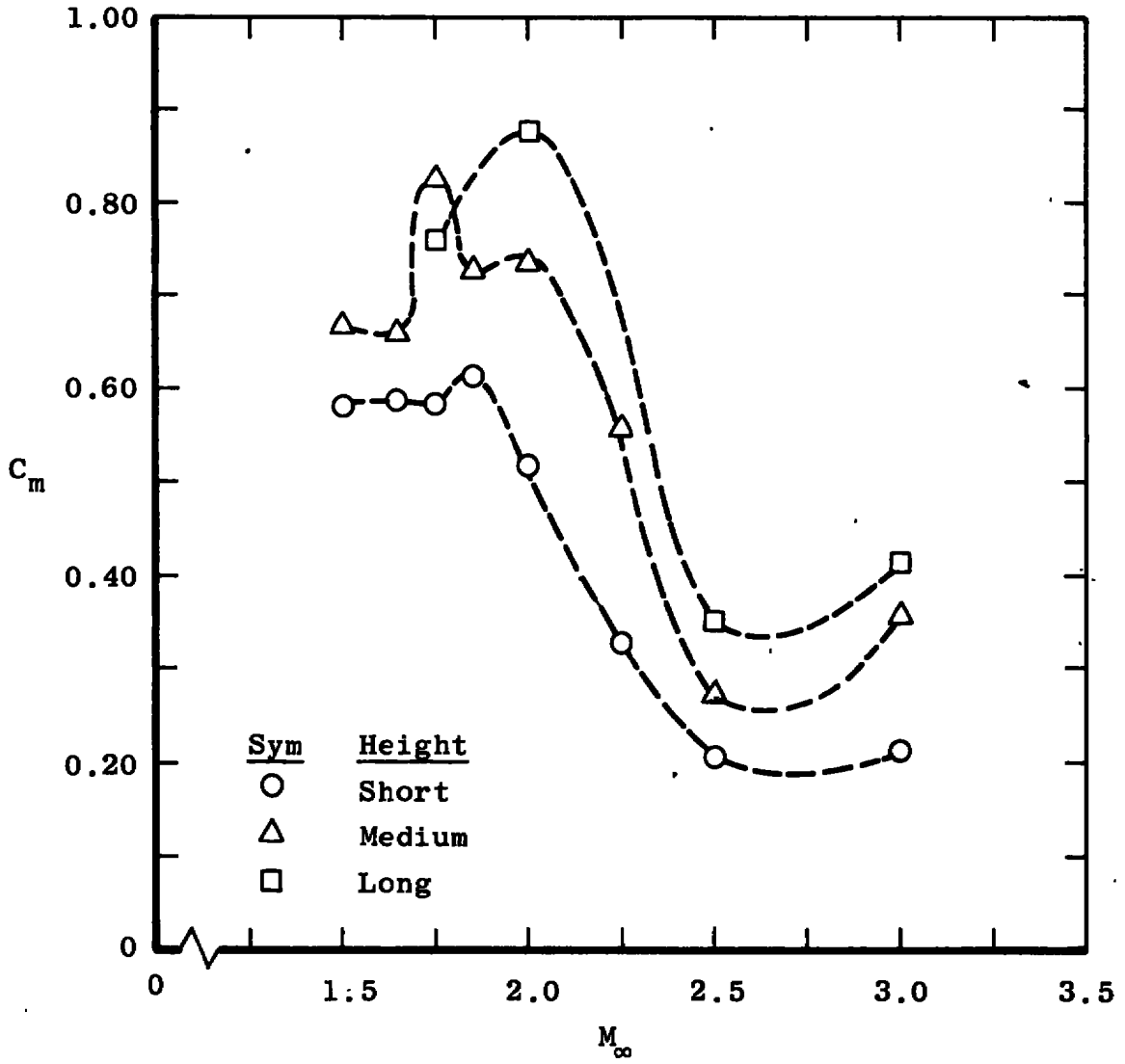


c. C_{A_t} versus M_∞
 Figure 15. Concluded.

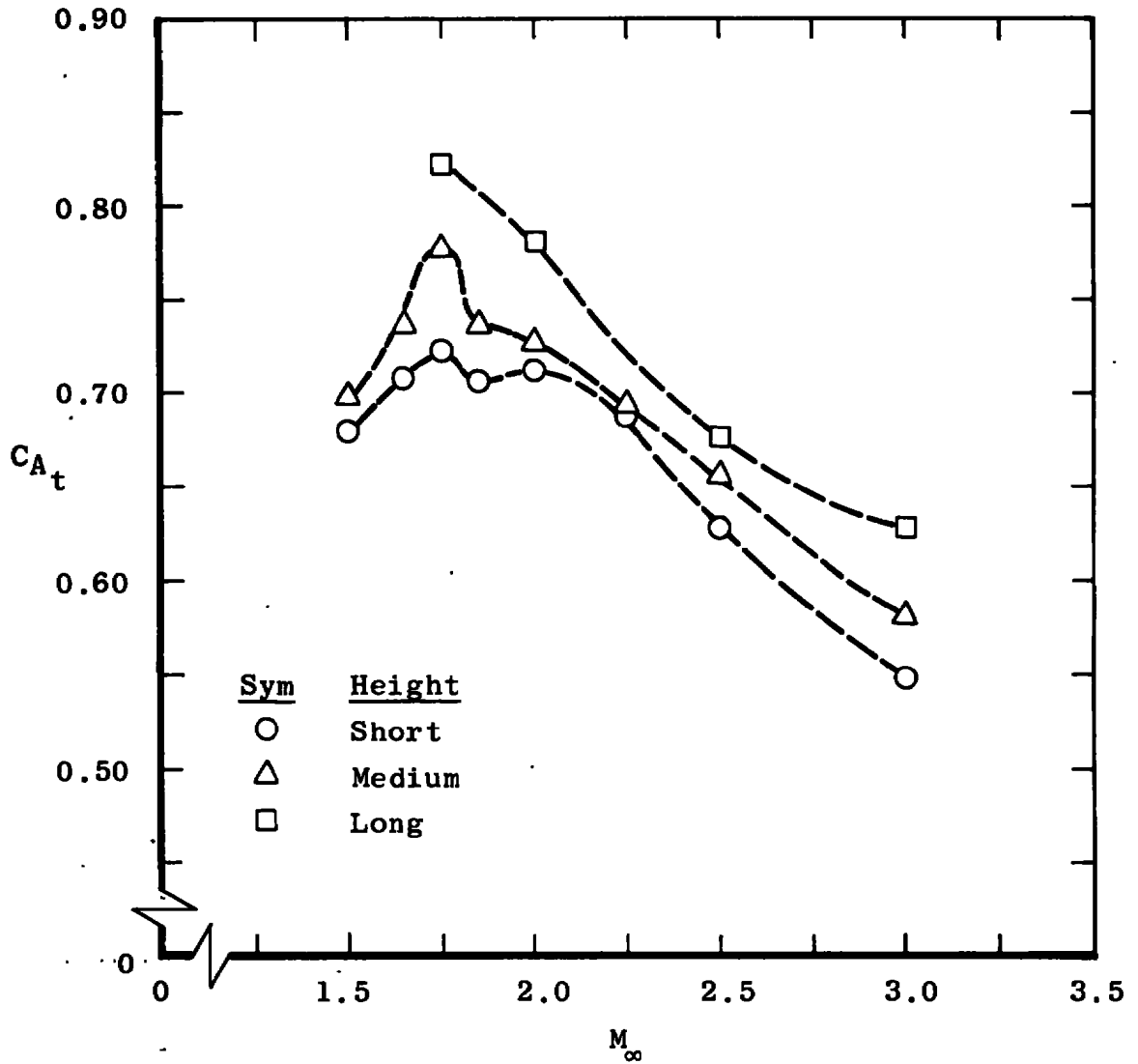


a. C_N versus M_∞

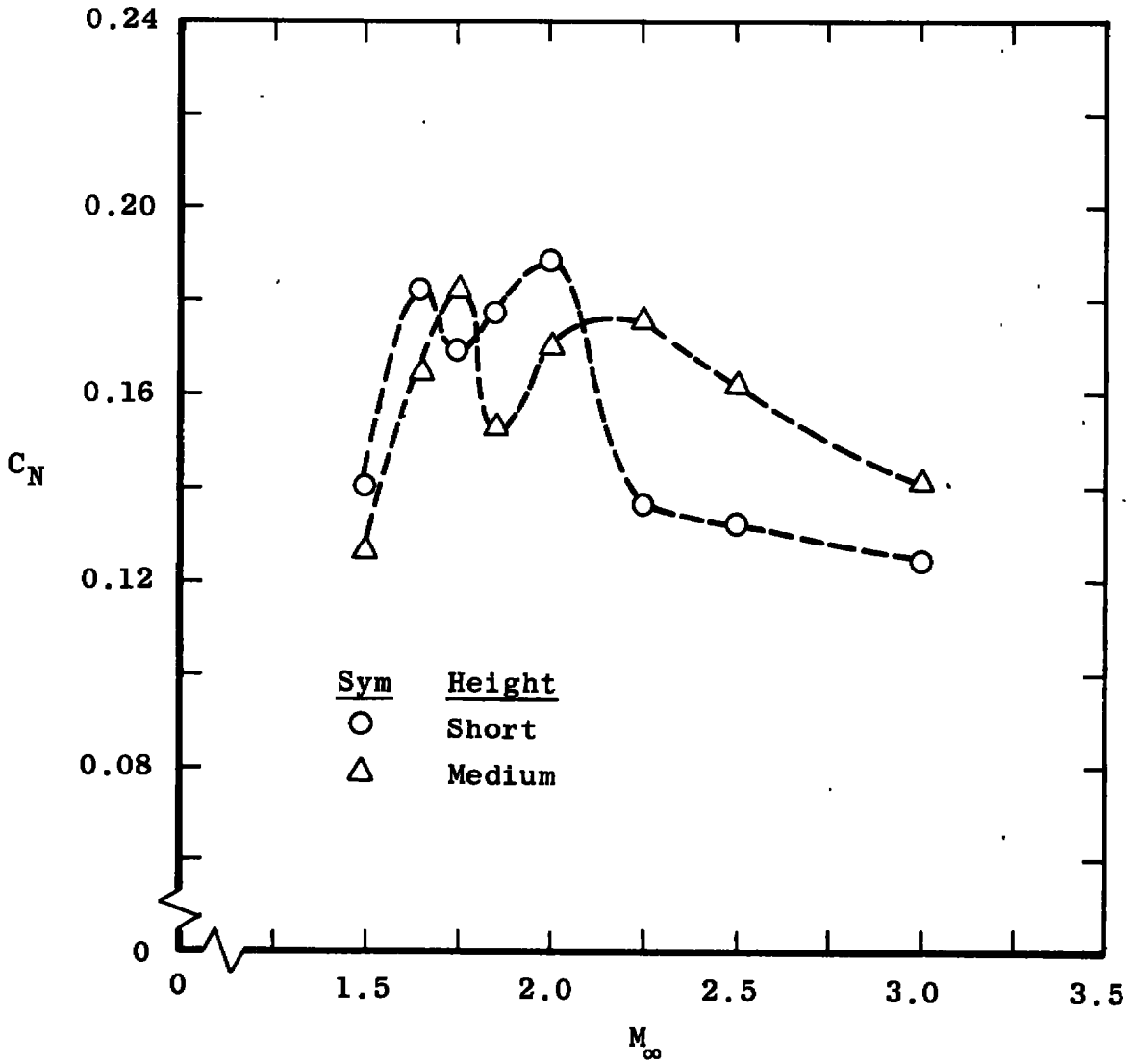
Figure 16. Effect of slipper height on the long cone with slippers in the forward position (X.3.1.2.1).



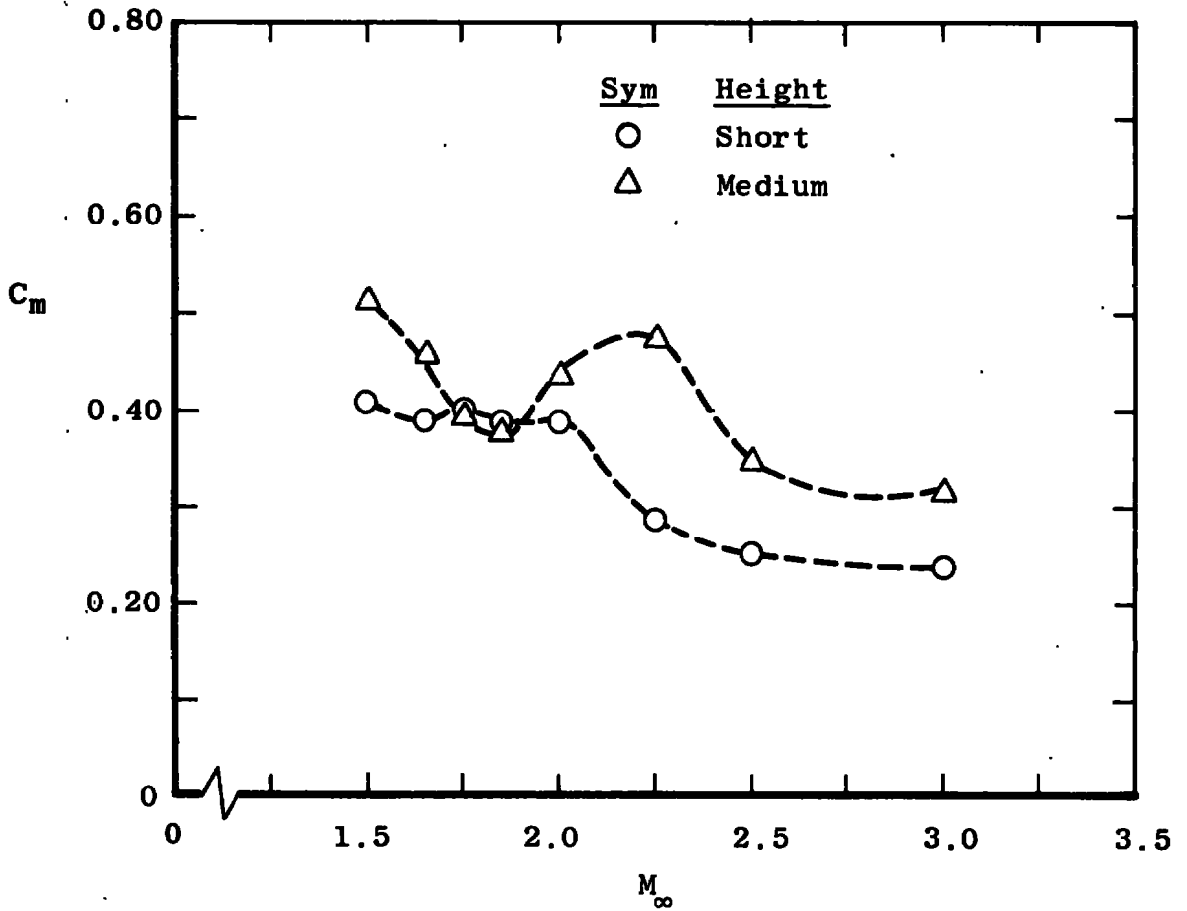
b. C_m versus M_∞
 Figure 16. Continued.



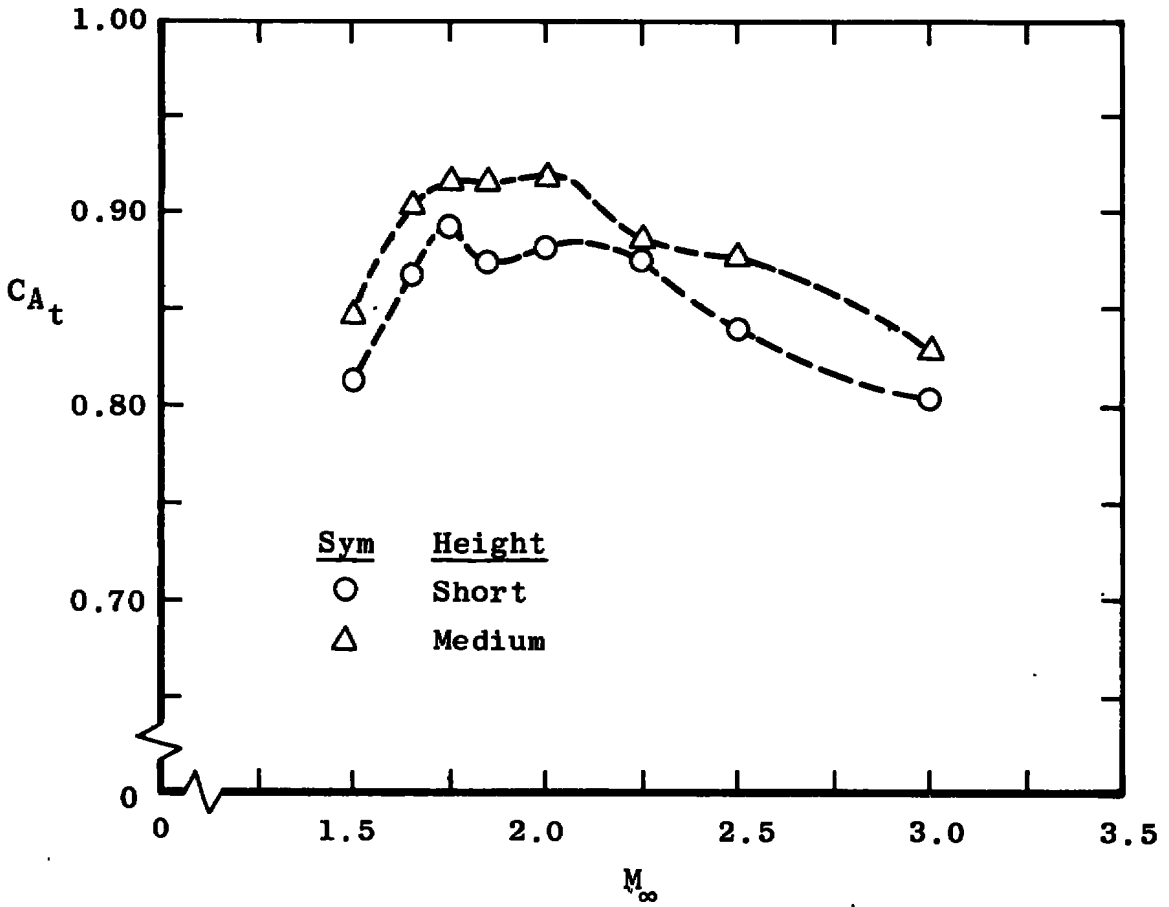
c. C_{A_t} versus M_∞
Figure 16. Concluded.



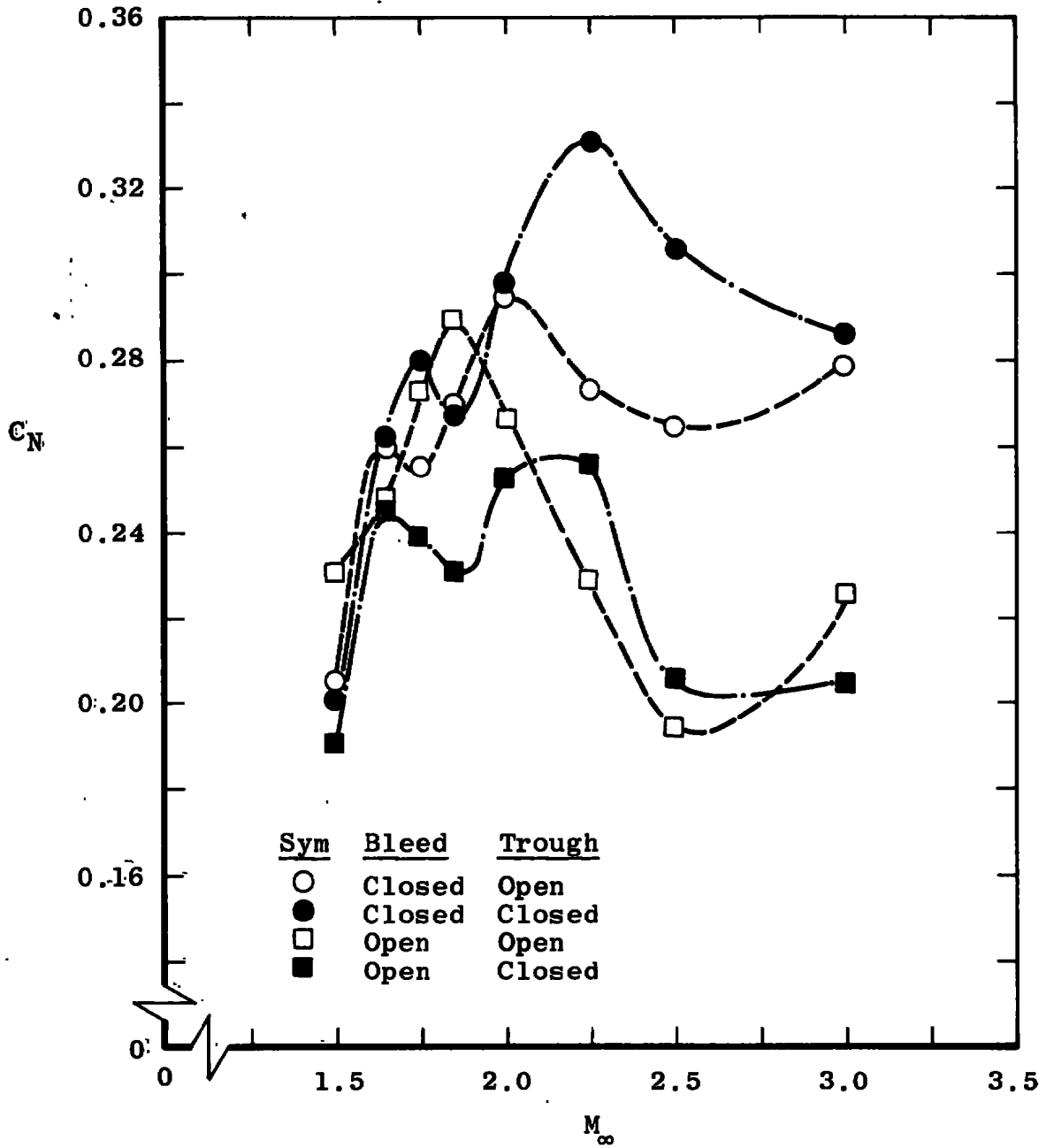
a. C_N versus M_∞
 Figure 17. Effect of slipper height on the blunt cone with slippers in the forward position (X.3.1.3.1).



b. C_m versus M_∞
Figure 17. Continued.

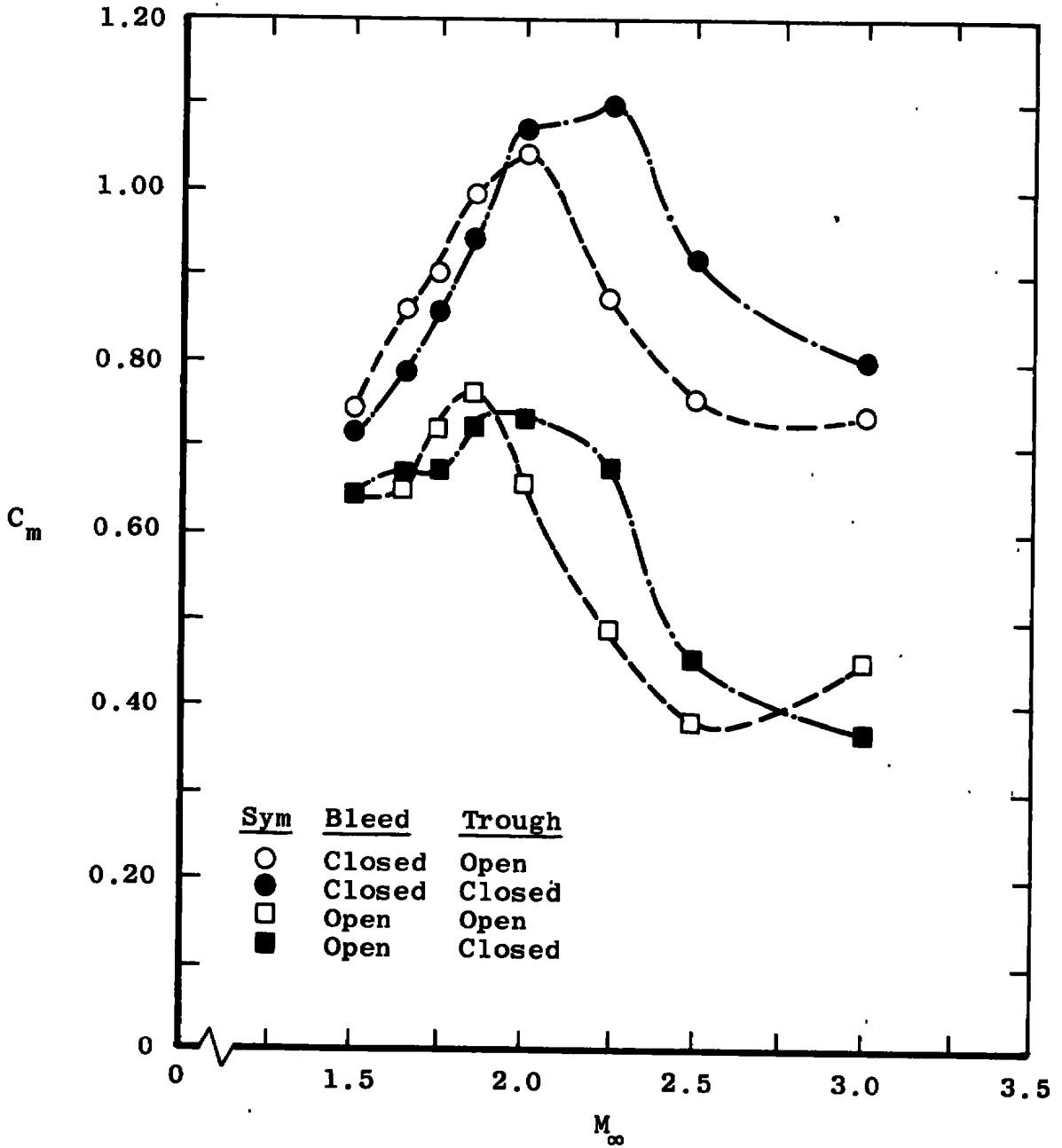


c. C_{A_t} versus M_∞
 Figure 17. Concluded.

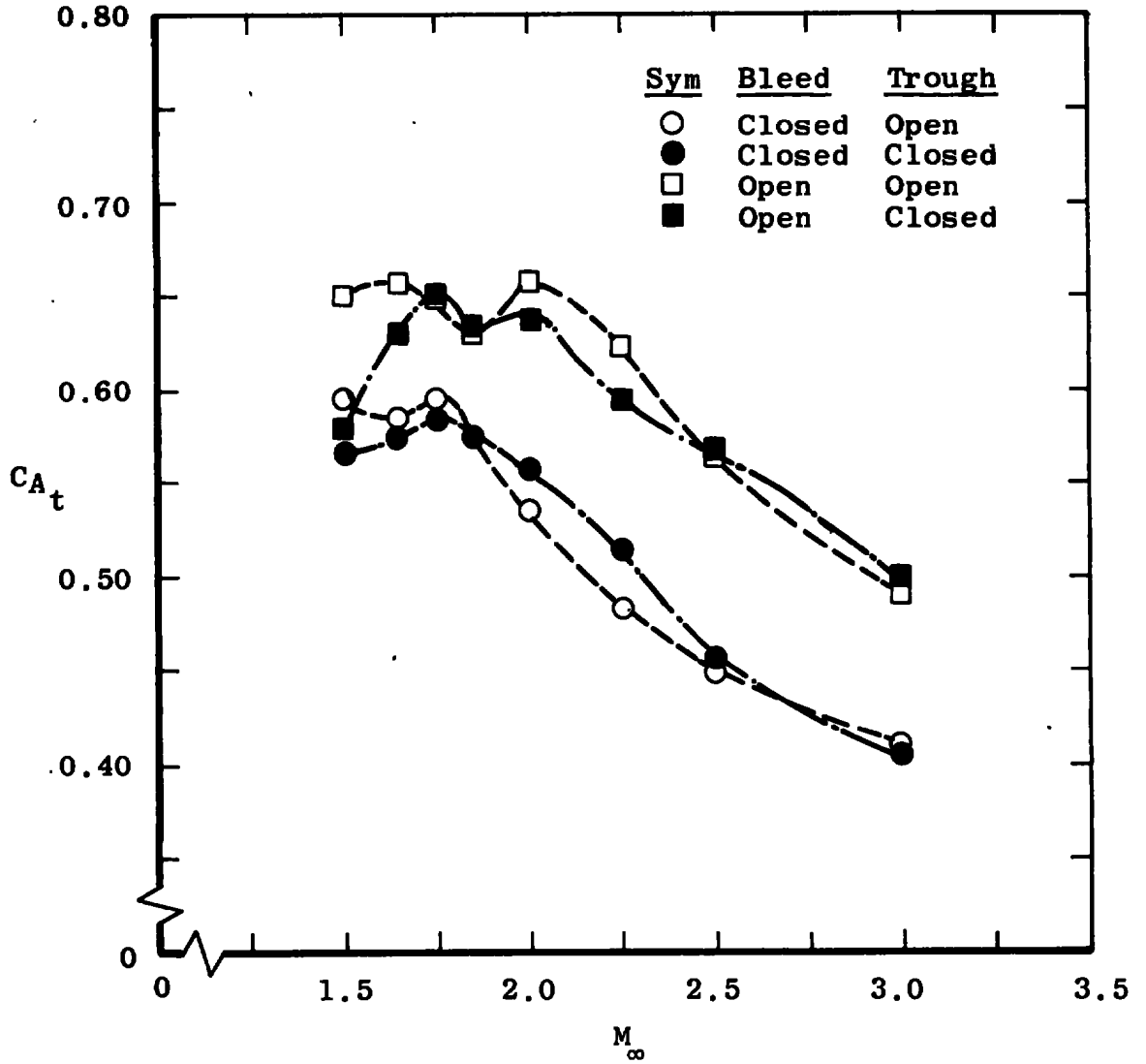


a. C_N versus M_∞

Figure 18. Effect of water trough and bleed area on long cone configuration with short slippers in the forward position (1.3X.2.2x).



b. C_m versus M_∞
 Figure 18. Continued.



c. C_{A_t} versus M_∞
 Figure 18. Concluded.

Table 1. Test Summary

Configuration**	Mach Number									
	1.50	1.65	1.75	1.85	2.00	2.25	2.50	3.00	3.50	4.00
1.3.2.2.2	0.7*	0.7	0.6	0.6	0.6	0.7	0.9	1.0		
1.3.1.2.2	0.8	0.9	0.9	0.8, 0.9	0.9	1.0	1.1	1.4		
1.3.1.2.1	0.8	0.8	0.8	0.8	0.8	0.8	1.0	1.2	1.2	1.3
1.3.1.3.1	0.7	0.7	0.6	0.7	0.6	0.7	0.7	0.9	1.1	1.3
1.1.1.3.1	0.6	0.6	0.6	0.7	0.6	0.6	0.7	0.9		
1.1.1.2.1	0.8	0.8	0.8	0.8	0.8	0.9	1.0	1.3		
2.1.1.2.1	0.8	0.8	0.7	0.8	0.8	0.9	1.0	1.2		
2.2.1.2.1	0.8	0.8	0.7	0.8	0.8	0.9	1.0	1.2		
2.3.1.2.1	0.8	0.8	0.7	0.8	0.8	0.9	0.9	1.2		
2.3.1.3.1	0.7	0.6	0.6	0.6	0.6	0.7	0.7	0.9		
3.3.1.2.1			0.6		0.7		0.8	0.7		
3.1.1.2.1	0.7	0.6	0.7	0.6	0.7	0.8	0.8	1.1		
1.3.2.2.2c	0.8	0.7	0.7	0.6	0.6	0.6	0.7	1.0		
1.3.1.2.2c	0.9	0.9	0.8	0.8	0.9	1.0	1.1	1.4		
1.1.1.2.2								1.2		
0.0.1.2.1	0.5, 0.6	0.6	0.7	0.7	0.9					

*Numbers in Table Are Nominal Test $Re_{\infty d} \times 10^{-6}$

**Identification of Model Configuration Nomenclature

First (Left Hand) Digit - Slipper Height (measured from centerline of model to inside top of slipper)

1. Short - 1.508 in. 2. Medium - 1.676 in. 3. Long - 1.806 in.

Second Digit - Forward Slipper Location (measured from center of aft slipper to center of forward slipper)

1. Aft - 8.08 in. 2. Mid - 9.18 in. 3. Forward - 10.27 in.

Third Digit - Bleed Area

1. Open 2. Closed

Fourth Digit - Nose Shape

1. Short Cone (Not Tested) 2. Long Cone 3. Blunt Cone

Fifth Digit - Brake

1. On 2. Off

If "c" appears after configuration number, water trough is closed.
In the data figures, X denotes the component that was varied.

NOMENCLATURE

A_b	Cross-sectional area at the base, 7.514 in. ²
b	Distance between rail centerlines, 2.200 in.
C_A	Forebody axial force coefficient, ($C_{A_t} - C_{A_b}$)
C_{A_b}	Base axial force coefficient, $-C_{p_b}(A_b/S)$
C_{A_t}	Total axial force coefficient, total axial force/ $q_\infty S$
C_m	Pitching moment coefficient, pitching moment/ $q_\infty Sd$
C_N	Normal force coefficient, normal force/ $q_\infty S$
C_{p_b}	Base pressure coefficient, $(p_b - p_\infty)/q_\infty$
d	Diameter of rocket sled, 3.00 in.
M_∞	Free-stream Mach number
p_b	Average base pressure, psia
p_∞	Free-stream static pressure, psia
p_0	Free-stream stagnation pressure, psia
q_∞	Free-stream dynamic pressure, psia
$Re_{\infty d}$	Free-stream Reynolds number based on model diameter
S	Projected frontal area of model, 8.289 in. ²
T_0	Free-stream stagnation temperature, °R